



# MAX-DOAS measurements of NO<sub>2</sub>, HCHO and CHOCHO at a rural site in Southern China

X. Li<sup>1,2</sup>, T. Brauers<sup>2</sup>, A. Hofzumahaus<sup>2</sup>, K. Lu<sup>1,2</sup>, Y. P. Li<sup>1,2</sup>, M. Shao<sup>1</sup>, T. Wagner<sup>3</sup>, and A. Wahner<sup>2</sup>

<sup>1</sup>College of Environmental Sciences and Engineering, Peking University, Beijing, China

<sup>2</sup>Institute for Energy- and Climate Research (IEK-8), Forschungszentrum Jülich, Jülich, Germany

<sup>3</sup>Max-Planck-Institut für Chemie, Mainz, Germany

Correspondence to: T. Brauers (th.brauers@fz-juelich.de)

Received: 12 January 2012 – Published in Atmos. Chem. Phys. Discuss.: 3 February 2012

Revised: 4 February 2013 – Accepted: 14 February 2013 – Published: 25 February 2013

**Abstract.** We performed MAX-DOAS measurements during the PRIDE-PRD2006 campaign in the Pearl River Delta region (PRD), China, for 4 weeks in July 2006 at a site located 60 km north of Guangzhou. The vertical distributions of NO<sub>2</sub>, HCHO, and CHOCHO were independently retrieved by an automated iteration method. The NO<sub>2</sub> mixing ratios measured by MAX-DOAS showed reasonable agreement with the simultaneous, ground based in-situ data. The tropospheric NO<sub>2</sub> vertical column densities (VCDs) observed by OMI on board EOS-Aura satellite were higher than with those by MAX-DOAS. The 3-D chemical transport model CMAQ overestimated the NO<sub>2</sub> VCDs as well as the surface concentrations by about 65 %. From this observation, a reduction of NO<sub>x</sub> emission strength in CMAQ seems to be necessary in order to well reproduce the NO<sub>2</sub> observations. The average mixing ratios of HCHO and CHOCHO were 7 ppb and 0.4 ppb, respectively, higher than in other rural or semirural environments. The high ratio of 0.062 between CHOCHO and HCHO corresponds to the high VOCs reactivity and high HO<sub>x</sub> turnover rate consistent with other observations during the campaign.

and the pointing direction of the telescope). The slant column density (SCD), which is the concentration of a species integrated along the paths where the registered photons traveled, can be derived from a DOAS fit. Despite the simplicity of the experimental setup, the conversion from measured SCDs to trace gas concentrations or profiles is a demanding task. As illustrated in Table 1, along with the numerous MAX-DOAS applications in the past decades, different methodologies for deriving the trace gas concentrations have been developed. The geometric approach, which is based on the assumption that the last scattering of a photon happens above the absorber layer, was used for estimating the trace gas concentrations in remote areas (Leser et al., 2003). However, for MAX-DOAS observations in the UV or at high aerosol loads the single scattering assumption is not valid. Under these conditions, radiative transfer models (RTMs) are required to derive trace gas profiles from measured SCDs. The different RTMs (see Table 1) calculate SCDs for trace gases on the basis of trace gas profiles as input to the model. In order to optimize the model input an inversion method is needed. This can either be optimal estimation (Rodgers, 2000) or an iteration procedure as presented by Pikel'naya et al. (2007). Both algorithms consist of two steps, i.e. first the aerosol extinction profile is retrieved from the measured oxygen dimer (O<sub>4</sub>) absorptions, then the trace gas profile is retrieved from the measured trace gas absorptions taking the aerosol extinction profile into account. Given that routine MAX-DOAS measurements often generate large data sets, an automated inversion method (e.g., Irie et al., 2011) is highly preferable. Inherently, only 2–3 independent pieces of profile information can be retrieved from the MAX-DOAS measurements.

## 1 Introduction

Multi-axis differential optical absorption spectroscopy (MAX-DOAS) is an effective remote sensing method for measuring tropospheric trace gases such as SO<sub>2</sub>, HCHO, NO<sub>2</sub>, CHOCHO (Irie et al., 2011; Wagner et al., 2011, and references therein). MAX-DOAS uses scattered sunlight at different elevation angles  $\alpha$  (i.e. the angle between horizon

**Table 1.** Overview of MAX-DOAS trace gas measurements.

Location	Period	# <sup>a</sup>	Species	RTM	Methodology	Ref.
Alert, Canada	Apr–May 2000	6	BrO	–	Geometric approach	1
Atlantic Ocean	Oct 2000	6	NO <sub>2</sub> , BrO	–	Geometric approach	2
Montserrat island	May 2002	10	SO <sub>2</sub> , BrO	–	Geometric approach	3
Ny-Ålesund Svalbard	Jul 2002	5	NO <sub>2</sub>	SCIATRAN	Predefined trace gas profile + RTM calculation	4
Po-valley, Italy	Sep 2003	5	HCHO	SCIATRAN	Manual iteration method	5
Cambridge & Gulf of Maine, USA	Jul–Aug 2004	5	NO <sub>2</sub> , HCHO, CHOCHO	TRACY	Manual iteration method	6
Reunion Island	Aug 2004–Jun 2005	5	BrO	DISORT	Predefined profiles + OEM <sup>b</sup>	7
Mount Tai, China	Jun 2006	5	HCHO, NO <sub>2</sub>	MCARaTS	Parametrized profile + OEM	8
Cabauw, Netherlands	Jun–Jul 2009	6	SO <sub>2</sub> , HCHO, NO <sub>2</sub> , CHOCHO	MCARaTS	Parametrized profile + OEM	9
Po-valley, Italy	Sep 2003	5	HCHO, NO <sub>2</sub>	McArtim	Parametrized profile + LMA <sup>c</sup>	10
Pearl River Delta, China	Jul 2006	7	NO <sub>2</sub> , HCHO, CHOCHO	McArtim	Parametrized profile + LMA	11

<sup>a</sup> Number of elevation angles, <sup>b</sup> Optimal Estimation Method, <sup>c</sup> Levenberg-Marquardt Algorithm

<sup>1</sup> Hönninger and Platt (2002), <sup>2</sup> Leser et al. (2003), <sup>3</sup> Bobrowski et al. (2003) <sup>4</sup> Wittrock et al. (2004), <sup>5</sup> Heckel et al. (2005), <sup>6</sup> Pikelnaya et al. (2007); Sinreich et al. (2007), <sup>7</sup> Theys et al. (2007), <sup>8</sup> Inomata et al. (2008); Irie et al. (2008), <sup>9</sup> Irie et al. (2011), <sup>10</sup> Wagner et al. (2011), <sup>11</sup> this work.

Therefore, during the inversion process, either a-priori information on the profile needs to be provided or a profile parameterization needs to be applied based on assumptions on the profile shape. Recent studies have compared the MAX-DOAS measured trace gas (e.g. NO<sub>2</sub>, HCHO) concentrations in the boundary layer to those obtained by in-situ techniques. In general, the differences were within 30 % (Pikelnaya et al., 2007; Inomata et al., 2008; Irie et al., 2011; Wagner et al., 2011). In addition, MAX-DOAS can serve as a tool to validate satellite-borne trace gas observations. The differences between MAX-DOAS and satellite measured NO<sub>2</sub> tropospheric vertical column densities were found to be 10–50 % for selected regions (Irie et al., 2008; Brinksma et al., 2008).

With the fast economic growth, the air quality has been of increasing concern in the Pearl River Delta (PRD) region in Southern China. In the last years, PRD was identified by satellite measurements as one of the “hot-spots” of NO<sub>2</sub>, HCHO, and CHOCHO (Richter et al., 2005; Wittrock et al., 2006; Vrekoussis et al., 2009). The observed high NO<sub>2</sub> levels reflect the prevailing anthropogenic emission sources, e.g. vehicles and industrial sources. Since HCHO and CHOCHO are mainly produced through the oxidation of volatile organic compounds (VOCs), their high concentration levels indicate the large photochemical turnover in the PRD atmosphere. However, only a few ground-based HCHO and CHOCHO measurements were reported for this region. During the PRIDE-PRD2006 field campaign, we performed one month of continuous MAX-DOAS observations for O<sub>4</sub>, NO<sub>2</sub>, HCHO, and CHOCHO. An automated aerosol retrieval method using O<sub>4</sub> absorption was developed, and the retrieved aerosol extinction agreed well with the total aerosol scattering measured by a nephelometer (Li et al., 2010). Here, we present the retrieval method and results for NO<sub>2</sub>, HCHO, and CHOCHO concentrations. These results are discussed with respect to simultaneously measured in-situ data, satellite observations, and chemical transport model simulations.

## 2 Experimental

### 2.1 Field campaign and measurement site

The PRIDE-PRD2006 field campaign took place in July 2006 in the Pearl River Delta (PRD) region in Southern China within the framework of the “Program of Regional Integrated Experiments of Air Quality over the Pearl River Delta” (PRIDE-PRD2006). The campaign focused on photochemistry and the formation of secondary pollutants like ozone and particles (Zhang et al., 2012). The MAX-DOAS measurements were conducted at one of the campaign supersites Back Garden (BG) located 23.50° N and 113.03° E. The BG site is approximately 60 km NW of downtown Guangzhou. It is located next to a water reservoir and is surrounded by farmland and small forests. During the campaign, the local traffic was quite limited. However, road works, building constructions, and biomass and cable burning were occasionally observed in the surrounding areas. The biomass and cable burning events were intense and prevailing in the period between 23 July and 25 July leading to high concentrations of aerosols and trace gases (Garland et al., 2008; Lou et al., 2010). The entire campaign was characterized by tropical weather conditions with high temperatures (28–36 °C) and high humidities (60–95 % RH). Extended rainfall occurred in periods influenced by typhoons Bilis (15–18 July) and Kaemi (26–29 July). The wind speed at BG site was usually low (less than 2 m s<sup>-1</sup>) in most of the time, which is a typical situation for inland areas in PRD during summer time (Fan et al., 2011). Such meteorological conditions favor the formation and accumulation of air pollution. High OH radical concentrations with noontime peak values of (1.5–2.6) × 10<sup>7</sup> cm<sup>-3</sup> as well as high OH reactivities *k*<sub>OH</sub> with values between 20 s<sup>-1</sup> and 120 s<sup>-1</sup> were observed at the BG site during the campaign (Lou et al., 2010; Lu et al., 2012). These observations indicate a strong photochemical processing compared to those in other places in the world.

A comprehensive suite of instruments was simultaneously operated at the BG supersite for the characterization of trace gases (Hua et al., 2008; Hofzumahaus et al., 2009; Lou et al., 2010; Lu et al., 2012; Li et al., 2011) and aerosols (Garland et al., 2008; Li et al., 2010; Yue et al., 2010; Xiao et al., 2011) in the local atmosphere. Measurements of  $\text{NO}_x$ ,  $\text{O}_3$ ,  $\text{SO}_2$ ,  $\text{H}_2\text{O}_2$ ,  $\text{CO}$ ,  $\text{CH}_4$ , C3-C12 VOCs,  $\text{CH}_3\text{OOH}$ ,  $\text{HCHO}$ ,  $\text{CHOCHO}$ , aerosol physical and chemical properties, and photolysis frequencies were performed on top of a hotel building (10 m a.g.l.) which was exclusively used by the measurement team.  $\text{OH}$ ,  $\text{HO}_2$ ,  $\text{HONO}$ , and  $\text{OH}$  reactivities were measured on top of a two stacked sea containers located about 200 m away from the hotel building. Detailed information with respect to the instrumentations, the accuracy and precision of the measurements can be found in Hofzumahaus et al. (2009), Yue et al. (2010), and Li et al. (2011).

## 2.2 MAX-DOAS

Our MAX-DOAS measurements were conducted by a commercial Mini-MAX-DOAS instrument (Fa. Hoffmann, Rauenberg, Germany). Since the instrument setup was described in detail by Li et al. (2010), only a brief outline follows. The Mini-MAX-DOAS instrument was installed on top of the hotel building, pointing East. It uses a miniature crossed Czerny-Turner spectrometer unit USB2000 (Ocean Optics Inc.) for spectrum recording. The spectrometer covers the spectral range of 292 nm to 443 nm with a spectral resolution of  $\approx 0.7$  nm full width at half maximum (FWHM). The scattered sunlight was collected and focused by a quartz lens and was led into the spectrometer unit by a quartz fiber bundle. A step motor was used for adjusting the viewing direction to a desired elevation angle  $\alpha$ , i.e.  $90^\circ$ ,  $30^\circ$ ,  $20^\circ$ ,  $15^\circ$ ,  $10^\circ$ ,  $5^\circ$ , and  $3^\circ$ . During daytime, one measurement cycle consisted of the sequential recording of the scattered sunlight spectrum at the seven elevation angles and took 10–15 min. For each spectrum, a constant signal level (i.e. 80 % of the saturation of the detector) was achieved by adjusting the integration time. During night, the instrument was set to record dark current and offset spectra. A fully automated program (MiniMax, Udo Friess, University of Heidelberg) was employed for the MAX-DOAS measurements.

The differential slant column density (DSCD) is defined as the difference of the slant column density (SCD) between  $\alpha \neq 90^\circ$  and  $\alpha = 90^\circ$  (c.f. Wagner et al., 2011). DSCDs of  $\text{NO}_2$ ,  $\text{HCHO}$ , and  $\text{CHOCHO}$  were determined by DOAS fit in the wavelength range where they have prominent absorptions. Figure 1 illustrates an example of the DOAS fit for the spectrum recorded on 19 July 2006 at 10:59, at a solar zenith angle of  $23^\circ$  and an elevation angle of  $3^\circ$ . For each measurement cycle, the corresponding zenith spectrum ( $\alpha = 90^\circ$ ) was taken as Fraunhofer reference spectrum (FRS) for the off-axis elevation angles (i.e.  $\alpha \neq 90^\circ$ ). This largely eliminates the stratospheric contributions to the DSCDs. The Ring spectrum was calculated from each measured spectrum (Busse-

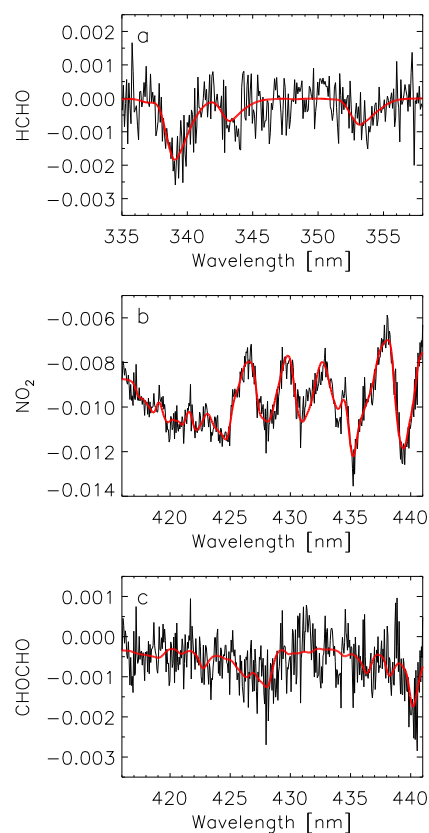


**Fig. 1.** Example of DOAS fit results for (a)  $\text{HCHO}$ , (b)  $\text{NO}_2$ , and (c)  $\text{CHOCHO}$ . The evaluated spectrum was recorded on 19 July 2006 at 10:59 LT, at  $\alpha = 3^\circ$ . Red line represents the fitted reference spectrum. Black line is the fit residual plus the absorption of the target species. Detailed settings of the DOAS fit are listed in Table S1 in the Supplement.

mer, 1993). For the fit of the absorbing trace gases, we used high resolution absorption cross sections which were convolved with the wavelength dependent instrument's slit function to match the resolution of the instrument (except for the  $\text{O}_4$  spectrum which was interpolated). These references include  $\text{HCHO}$  (Meller and Moortgat, 2000),  $\text{BrO}$  (Wilmouth et al., 1999),  $\text{CHOCHO}$  (Volkamer et al., 2005),  $\text{H}_2\text{O}$  (Rothman et al., 2005),  $\text{NO}_2$  (Voigt et al., 2002),  $\text{O}_3$  at 280 K (Voigt et al., 2001), and  $\text{O}_4$  (Greenblatt et al., 1990) with a manual adjustments of wavelength axis (R. Sinreich, personal communication, 2007). In addition, the solar  $\text{I}_0$ -effect (Platt et al., 1997) was corrected for  $\text{NO}_2$  and  $\text{O}_3$  reference spectra with slant column density of  $1.5 \times 10^{17} \text{ cm}^{-2}$  and  $1.5 \times 10^{20} \text{ cm}^{-2}$ , respectively. The wavelength calibration and the wavelength dependent instrument's slit function were calculated from a fit of the measured Fraunhofer reference spectra to a high resolution Fraunhofer spectrum (Kurucz et al., 1984). It should be noted that in the first version of our manuscript (Li et al., 2012) we used a constant slit

**Table 2.** Parameter settings of RTM calculations for NO<sub>2</sub>, HCHO, and CHOCHO DSCDs.

Parameter	Value		
	NO <sub>2</sub>	HCHO	CHOCHO
Wavelength	435 nm	339 nm	440 nm
Surface albedo		7 %	
Single scattering albedo (SSA)		0.85	
Asymmetry factor (g)		0.68	
Aerosol profile	from O <sub>4</sub> DSCDs at 360 nm <sup>a</sup>		
O <sub>3</sub> profile	USSA <sup>b</sup> filled with 40 ppb from 0–1 km		
<i>T</i> and <i>P</i> profiles	USSA		
NO <sub>2</sub> profile	0–15 km: from NO <sub>2</sub> DSCDs at 435 nm > 15 km: USSA		

<sup>a</sup> see Li et al. (2010)<sup>b</sup> US Standard atmosphere

function to calculate the references which led to different values for all trace gases.

The conversion from measured DSCDs to tropospheric vertical column density (VCD) is usually done by the differential air mass factor (DAMF). The air mass factor (AMF) can be regarded as the path enhancement of SCD compared to VCD. DAMF is defined as the difference of air mass factor (AMF) between  $\alpha \neq 90^\circ$  and  $\alpha = 90^\circ$ . For photons received by the MAX-DOAS telescope, if their last scattering event happens above the trace gas layer, the AMF for the zenith and the off-axis view can be estimated as 1 and  $1/\sin\alpha$ , respectively. Thus, the trace gas tropospheric VCD can be written as

$$\text{VCD}_{\text{geo}} = \frac{\text{DSCD}_\alpha}{\text{DAMF}_\alpha} = \frac{\text{DSCD}_\alpha}{(1/\sin\alpha) - 1} \quad (1)$$

where  $\alpha$  is the elevation angle of the telescope. This method is called “geometric approach”. For photons received by the telescope at higher elevation angles, the probability of their last scattering event occurring above the trace gas layer is increased. Thus we calculated  $\text{VCD}_{\text{geo}}$  for NO<sub>2</sub>, HCHO, and CHOCHO from the corresponding DSCDs at the highest off-zenith elevation angle, i.e.  $\alpha = 30^\circ$ .

Compared to the simple geometric approach, the radiative transfer modeling of DSCDs is a demanding task. In this study, the DSCDs calculations were performed by McArtim, which is a backward Monte-Carlo RTM with the treatment of multiple scattering in a fully spherical geometry (Deutschmann et al., 2011). For each trace gas (NO<sub>2</sub>, HCHO, and CHOCHO), its vertical distribution was retrieved by iteratively adjusting the profile until the measured DSCDs best fit with the modeled DSCDs. The parameter settings of McArtim are listed in Table 2. Following Li et al. (2010), we used a two-layer setup for the trace gas distribution in the troposphere (0–15 km height). The trace gas concentrations (unit: cm<sup>-3</sup>) were assumed to be homogeneous in a layer near the ground surface (called mixing layer, ML), while the concentrations in the layer aloft (i.e. the free troposphere) decrease exponentially with height. This type of trace gas dis-

tribution was frequently observed in polluted regions (e.g., Fried et al., 2003; Junkermann, 2009; Klippel et al., 2011). The concentration profile  $c(z)$  can be described with a limited set of parameters

$$c(z) = \begin{cases} \text{VCD} \cdot F/H & z \leq H \\ \beta \cdot \exp(-z/\xi) & z > H \end{cases} \quad (2)$$

where  $z$  is the height above ground, VCD denotes the trace gas tropospheric vertical column density of the respective trace gas,  $F$  is the fraction of the  $\text{VCD}_{\text{rtm}}$  residing in the ML, and  $H$  is the height of ML.  $\beta$  is the normalization factor and  $\xi$  is the scaling height for the trace gas in the free troposphere. We performed test runs of the retrieval and found that the results were not sensitive to  $\xi$  under the conditions encountered here since most of the trace gas was present in the mixing layer. Thus  $\xi$  was set to a constant value of 5 km. The norm  $\beta$  is calculated from the integral of  $c(z)$  over the entire troposphere  $\text{VCD} = \int_0^{15 \text{ km}} c(z) dz$  leading to

$$\beta = \frac{(1 - F) \cdot \text{VCD}}{\xi (\exp(-H/\xi) - \exp(-15 \text{ km}/\xi))} \quad (3)$$

With the input given above, the McArtim program calculates the set of trace gas DSCDs ( $R_\alpha$ ) at the six elevation angles of the measurements. In order to achieve the best estimates for  $F$ ,  $H$ ,  $\text{VCD}_{\text{rtm}}$  (subscript rtm refers to the use of the RTM, in contrast to the geometric approach) we minimized

$$\chi^2(\text{VCD}_{\text{rtm}}, F, H) = \sum_{\alpha=30^\circ}^{30^\circ} \left( \frac{M_\alpha - R_\alpha(\text{VCD}_{\text{rtm}}, F, H)}{\sigma(M_\alpha)} \right)^2 \quad (4)$$

where  $M_\alpha$  represents the measured DSCDs. The weights are presented by the statistical error (precision) of the measured data,  $\sigma(M_\alpha)$ . In order to reduce the atmospheric variations as well as measurement noise of a single observation, the profile retrieval was applied to measured DSCDs averaged over one hour. The minimization procedure was conducted automatically using an implementation of the Levenberg-Marquardt algorithm (mpfit<sup>1</sup>, realized in IDL).

Since the PRD region is characterized by wide spread emission sources, most of the trace gases reside in the ML and the trace gas concentrations in the ML are much higher than those in the layer aloft. Therefore, the modeled DSCDs are not sensitive to change of  $\xi$  (see above), and values of  $F$  are close to 1. The three parameter ( $\text{VCD}_{\text{rtm}}$ ,  $F$ , and  $H$ ) retrieval yielded  $F > 0.95$  for almost all cloud-free periods. In addition, the statistical error of the retrieved  $F$  was large associated with a cross-correlation between  $F$  and  $H$ . Increasing  $H$  or decreasing  $F$  have the same effect on the modeled DSCDs. In order to overcome this issue, we finally fixed the values of  $F$  to 1; only VCD and  $H$  were retrieved. This approach resulted in a “box shape” profile. The trace

<sup>1</sup>C. B. Markwardt, mpfit – Robust non-linear least squares curve fitting, <http://cow.physics.wisc.edu/~craigm/idl/fitting.html>.

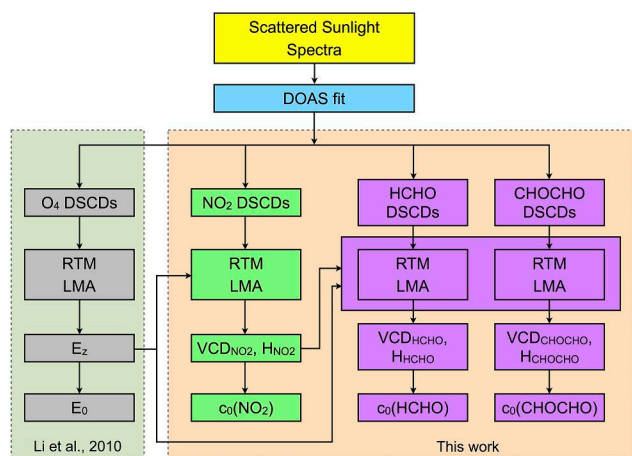


**Fig. 2.** Flow diagram of MAX-DOAS trace gas vertical distribution retrieval.

gas concentrations  $c_0$  are universal in the box and equal to  $VCD_{\text{rtm}}/H$ .  $c_0$  can then be compared to ground-based measurements which were done at the BG site.

Figure 2 depicts the flow diagram of the trace gas vertical distribution retrieval procedure. In order to well simulate the aerosol scattering effects by RTM, aerosol vertical distributions were retrieved beforehand from  $O_4$  DSCDs in the way as described by Li et al. (2010). The derived aerosol extinction profiles were used as input to the trace gas vertical distribution retrieval. The retrieval of  $NO_2$  vertical distribution was performed as the second step. Given the influence of  $NO_2$  absorption on the HCHO and CHOCHO DSCDs calculation (Table 3), the retrieved  $NO_2$  vertical distribution was used as RTM input during the vertical distribution retrieval for HCHO and CHOCHO. HCHO and CHOCHO vertical distributions were retrieved independently.

The errors of the retrieved trace gas vertical distribution consist of statistical errors which arise mainly from the uncertainty of the DSCDs, and systematic errors which originate from the uncertainty of the RTM input parameters and of the DSCD simulation. The statistical errors were derived from the mpfit procedure. Within RTM intercomparison activities (Hendrick et al., 2006; Wagner et al., 2007) the uncertainty of DSCD calculations by McArtim were found to be less than 10%. The sensitivities of the modeled DCSDs with respect to RTM input parameters are listed in Table 3. The surface albedo, the field of view of the telescope (FOV), and the surface  $O_3$  and  $NO_2$  have minor influences on the modeled DSCDs. The major uncertainty sources to the modeled DSCDs are the aerosol properties, namely the single scattering albedo (SSA), the asymmetry factor ( $g$ , under the Henyey-Greenstein approximation), and the aerosol optical depth (AOD). While the increase of SSA and  $g$  lead to a simultaneous increase of modeled DSCDs at all elevation angles, the increase of AOD results in a decrease of modeled DSCDs. It was found that 30% change of modeled DSCDs

results in  $\approx 25\%$  change of the retrieved  $VCD_{\text{rtm}}$  and  $c_0$ . During the campaign, the systematic errors of the measured SSA and AOD were 10% and 30%, respectively, and the uncertainty of  $g$  was 10% (Garland et al., 2008; Li et al., 2010). Therefore, we conclude that the total systematic error of the retrieved  $VCD_{\text{rtm}}$  and  $c_0$  are around 35%.

### 2.3 In-situ $NO_2$ measurement

In-situ  $NO_2$  concentrations were measured by a commercial instrument (Takegawa et al., 2006). The inlet of the sampling line was located on top of the hotel building.  $NO_2$  in the sampled air was converted to NO in a photolytical reactor (Droplet Measurement Technologies, Model BLC) with an conversion efficiency of 30%. The NO was then detected by NO- $O_3$  chemiluminescence (Thermo Electron, Model 42CTL). The 1 min detection limit for  $NO_2$  was 170 ppt, and the corresponding accuracy was 13%.

### 2.4 Numerical simulation of $NO_2$

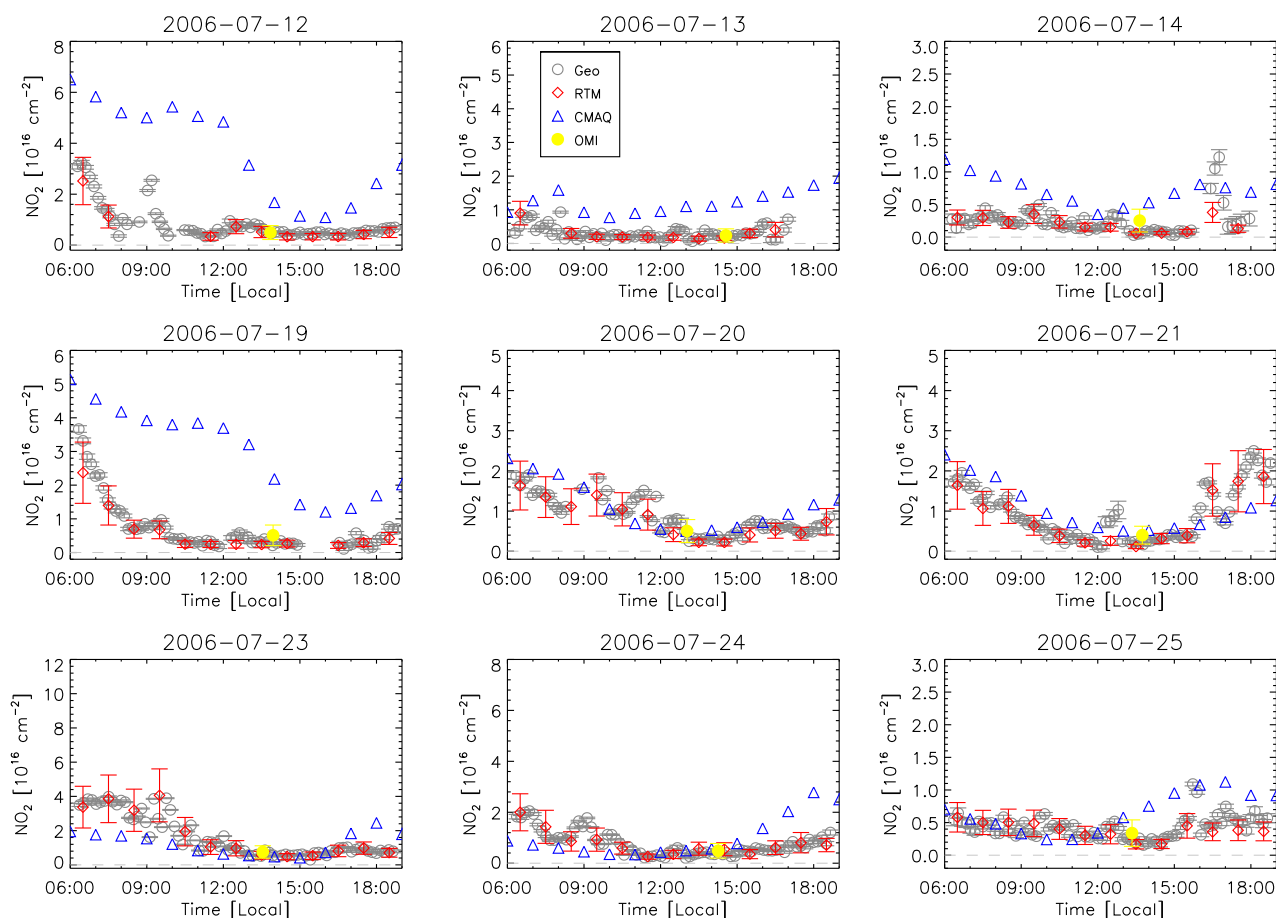
Model3-CMAQ version 4.5.1 was employed to simulate the  $NO_2$  concentrations during the period of the campaign. Details of the model configuration are described by Wang et al. (2010). The CMAQ model uses SAPRC99 as chemical mechanism, and is driven by MM5 for meteorology field and SMOKE for source emissions. The time step of the model was set to 1 h. There are three nested domains in the model system with grid spacing of 36 km, 12 km, and 4 km. All grids have 13 layers vertically extending from the surface to an altitude of 17 km above the ground, with seven layers below 1 km and the first layer thickness of 18 m. While the TRACE-P anthropogenic emission inventory was used for the 36 km domain, the emission inventories used for the 12 km domain and the 4 km domain were updated according to recent studies in PRD region (Zheng et al., 2009). Mobile sources and power generation point sources contribute about 47% and 39%, respectively, to the total  $NO_x$  emissions in PRD while mobile sources, evaporation losses of solvents and petroleum, and biogenic sources are the three largest contributors to VOC emissions, accounting for 38%, 24%, and 23%, respectively. Spatially, both  $NO_x$  and VOC emissions are concentrated over the inland urban areas of Guangzhou, Foshan, and Dongguan; the coastal areas of Dongguan and Shenzhen; and the urban core of Hong Kong.

## 3 Results

The MAX-DOAS instrument was operated for the campaign period from 3 July to 25 July 2006. However, as already discussed by Li et al. (2010), only 9 virtually cloud-free days were suitable for aerosol and trace gas vertical distribution retrieval. Measured DSCDs of  $NO_2$ , HCHO, and CHOCHO on these 9 days are displayed in Fig. S1 in the Supplement.

**Table 3.** Sensitivities of the RTM inputs on the calculated NO<sub>2</sub>, HCHO, and CHOCHO DSCDs.

	Surface albedo	FOV	SSA	g	AOD	NO <sub>2</sub> ( $\leq 1$ km)	O <sub>3</sub> ( $\leq 1$ km)
$\Delta$ Param.	+ 15 %	+ 0.1°	+ 10 %	+ 15 %	$\times 3$	$\times 10$	$\times 10$
$\Delta$ DSCDs							
NO <sub>2</sub>	+ 2.4 %	+ 0.4 %	+ 7.6 %	+ 9.3 %	- 47.7 %	-	- 0.04 %
HCHO	+ 1.8 %	+ 0.5 %	+ 6.8 %	+ 9.1 %	- 49.5 %	- 8.3 %	- 0.04 %
CHOCHO	+ 2.1 %	+ 0.3 %	+ 7.6 %	+ 10.9 %	- 49.3 %	- 10.1 %	- 0.01 %

**Fig. 3.** Time series of NO<sub>2</sub> vertical column densities (VCDs) on the 9 cloud-free days during the PRIDE-PRD2006 campaign. The grey circles represent NO<sub>2</sub> VCDs calculated by the geometric approach (i.e. Eq. 1), the red diamonds refer to NO<sub>2</sub> VCDs derived from the NO<sub>2</sub> vertical distribution retrieval (i.e. Fig. 2), the blue triangles are NO<sub>2</sub> VCDs calculated by the CMAQ model, and the yellow dots are NO<sub>2</sub> VCDs observed by OMI from space.

The vertical column densities using the RTM retrieval ( $VCD_{\text{rtm}}$ ) of NO<sub>2</sub>, HCHO, and CHOCHO are shown in Figs. 3–5. The mean values of  $VCD_{\text{rtm}}$  were  $7.2 \times 10^{15} \text{ cm}^{-2}$ ,  $1.5 \times 10^{16} \text{ cm}^{-2}$ , and  $1.2 \times 10^{15} \text{ cm}^{-2}$  for NO<sub>2</sub>, HCHO, and CHOCHO, respectively. The NO<sub>2</sub>  $VCD_{\text{rtm}}$  showed higher values around early morning before 09:00 LT (local time, LT = UTC + 8 h) and late afternoon (after 17:00 LT).  $VCD_{\text{rtm}}$  of HCHO and CHOCHO displayed similar diurnal variation patterns having their peak values at

around noon or late afternoon. Considering the measurement and retrieval errors, NO<sub>2</sub> VCDs calculated by the geometric approach ( $VCD_{\text{geo}}$ ) are nearly identical with the  $VCD_{\text{rtm}}$ . For the whole data set ( $N = 109$ ), the slopes  $B_0$  of a linear regression forced through the origin ( $VCD_{\text{geo}}$  versus  $VCD_{\text{rtm}}$ ) are  $1.06 \pm 0.14$  ( $R^2 = 0.95$ ) for NO<sub>2</sub> (Fig. S2). With respect to HCHO and CHOCHO, the geometric approach overestimated their VCDs, especially during early morning and late afternoon hours.  $B_0$  was found to be  $1.15 \pm 0.07$  ( $R^2 = 0.67$ )

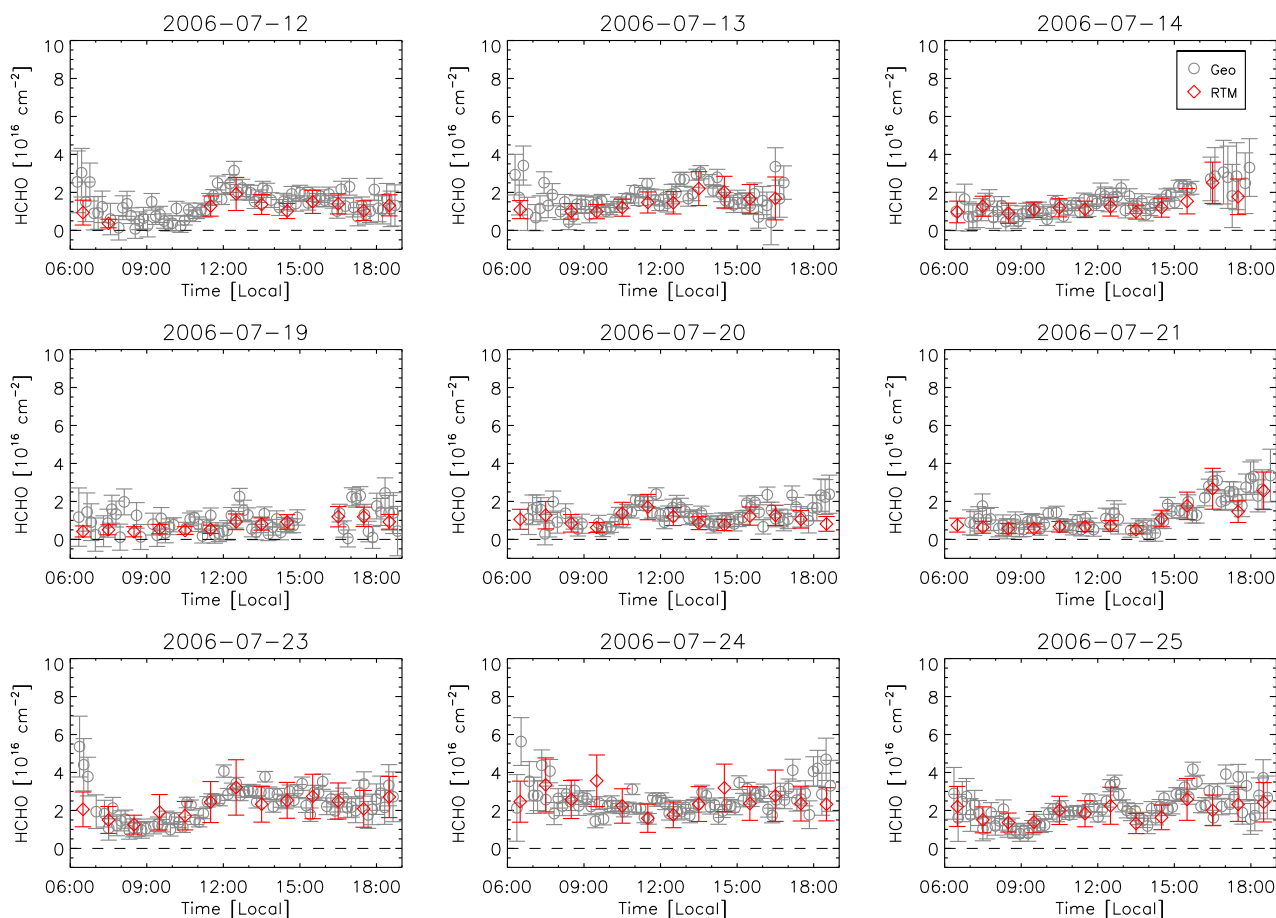


**Fig. 4.** Time series of HCHO vertical column densities (VCDs) on the 9 cloud-free days during the PRIDE-PRD2006 campaign. The grey circles represent HCHO VCDs calculated by the geometric approach (i.e. Eq. 1), and the red diamonds refer to HCHO VCDs derived from the HCHO vertical distribution retrieval (i.e. Fig. 2).

for HCHO (Fig. S3), and  $1.15 \pm 0.08$  ( $R^2 = 0.40$ ) for CHOCHO (Fig. S4), respectively.

The retrieved mixing layer heights  $H$  of the three trace gases are shown together with the  $H$  of aerosols (Li et al., 2010) in Fig. 6.  $H_{\text{NO}_2}$ ,  $H_{\text{HCHO}}$ ,  $H_{\text{CHOCHO}}$ , and  $H_{\text{aerosol}}$  showed similar diurnal variation patterns. In general,  $H$  was increasing after sunrise and started decreasing before sunset. Values of  $H_{\text{NO}_2}$  were lower than those of  $H_{\text{HCHO}}$ ,  $H_{\text{CHOCHO}}$ , and  $H_{\text{aerosol}}$ . In early morning hours, when  $H_{\text{NO}_2}$  was below 400 m,  $H_{\text{HCHO}}$ ,  $H_{\text{CHOCHO}}$ , and  $H_{\text{aerosol}}$  were in the range of 400 m to 1 km. While  $H_{\text{CHOCHO}}$  increased dramatically during the day and reached peak values of 2–4 km in the afternoon, peak values of  $H_{\text{NO}_2}$  and  $H_{\text{HCHO}}$  were usually below 2 km.

The trace gas mixing ratios (in ppb) at ground level can be calculated as  $m_0 = \text{VCD}/H \times M_0$  with  $M_0$  being the conversion factor from  $\text{cm}^{-3}$  to ppb. Figure 7 shows the time series of the derived  $\text{NO}_2$ , HCHO, and CHOCHO mixing ratios. The average daytime mixing ratios of  $\text{NO}_2$ , HCHO, and CHOCHO were 6.3 ppb, 7.0 ppb, and 0.4 ppb, respectively.

During the days 23 July–25 July when intense biomass and electric cable burning events occurred in the previous night in the surrounding areas, high levels of HCHO ( $\approx 20$  ppb) and CHOCHO ( $\approx 0.8$  ppb) were found in the early morning hours. In the same time periods,  $\text{NO}_2$  mixing ratios up to 40 ppb were observed by both MAX-DOAS and in-situ techniques. The mixing ratio of  $\text{NO}_2$  shows clear diurnal variation having its maxima in the early morning hours in all days. In contrast, the diurnal variations of the mixing ratios of HCHO and CHOCHO are less prominent. In most days, higher values of the mixing ratios of HCHO and CHOCHO were observed in morning hours. However, there are days (i.e. 20, 21, and 23 July) in which a slight increase of the CHOCHO mixing ratio was identified around noon. While the mixing ratio of  $\text{NO}_2$  varied in a similar way as its VCDs during the day, the variation of the HCHO and CHOCHO mixing ratio were to some extent opposite to their VCDs.

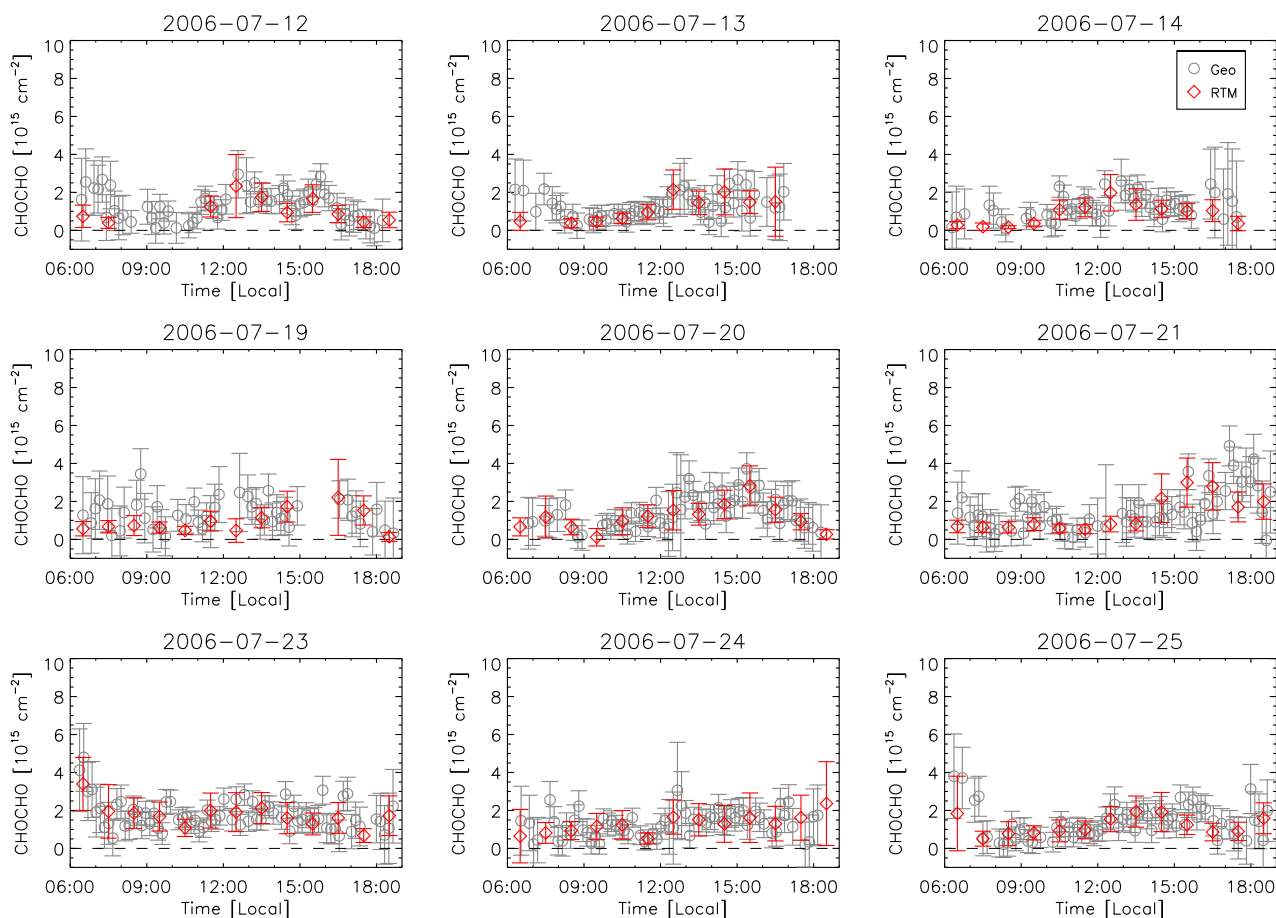


**Fig. 5.** Time series of CHOCHO vertical column densities (VCDs) on the 9 cloud-free days during the PRIDE-PRD2006 campaign. The grey circles represent CHOCHO VCDs calculated by the geometric approach (i.e. Eq. 1), and the red diamonds refer to CHOCHO VCDs derived from the CHOCHO vertical distribution retrieval (i.e. Fig. 2).

## 4 Discussion

### 4.1 NO<sub>2</sub>

During the campaign, we encountered high aerosol loads at BG site (Garland et al., 2008; Li et al., 2010). On the 9 cloud free days, the AOD measured by MAX-DOAS ranged from 0.15 to 4.18 with mean value of  $1.56 \pm 0.97$  (Li et al., 2010). Even though, good agreement between NO<sub>2</sub> VCD<sub>rtm</sub> and NO<sub>2</sub> VCD<sub>geo</sub> (Figs. 3 and S1) was found, indicating that the geometric approach is well suited for estimating the tropospheric NO<sub>2</sub> VCDs at the BG site. Similar results were found by Wagner et al. (2011) in the Po Valley area, i.e. differences between NO<sub>2</sub> VCD<sub>geo</sub> and VCD<sub>rtm</sub> were within 12%. However, different to Wagner et al. (2011), we did not observe a dependence of the relative difference between VCD<sub>rtm</sub> and VCD<sub>geo</sub> ( $\Delta\text{VCD} = (\text{VCD}_{\text{rtm}} - \text{VCD}_{\text{geo}})/\text{VCD}_{\text{rtm}}$ ) on the mixing layer height ( $H_{\text{NO}_2}$ ) at the BG site;  $\Delta\text{VCD}$  and  $H_{\text{NO}_2}$  are uncorrelated ( $R^2 = 0.01$ ). Since the differences between VCD<sub>geo</sub> and VCD<sub>rtm</sub> are rather small and in the order of the measurement and data retrieval uncertainties, no correlation

between  $\Delta\text{VCD}$  and other measured parameters can be expected.

Simultaneous in-situ NO<sub>2</sub> measurements can be used to validate the NO<sub>2</sub> mixing ratios derived from the MAX-DOAS observations. The scatter plot of NO<sub>2</sub> mixing ratios derived from MAX-DOAS vs. in-situ chemiluminescence data (Fig. 8) provides a high degree of correlation,  $R^2 = 0.83$  for a data set of  $N = 107$  simultaneous measurements. At this high degree of correlation, the slope  $B_0$ , forced through the origin, is  $0.88 \pm 0.14$ . Considering the errors in both coordinates, the goodness-of-fit parameter  $Q$  (cf. Press et al., 2007) equals 0.9 indicating that the scatter of the data points around the regression line can be explained by the measurement errors of both techniques. Here we included the fit error (usually small) and the errors of the SSA,  $g$ , and AOD, since these can vary with the different conditions during the campaign.

The 12% difference between MAX-DOAS and the in-situ technique is in line with those obtained by Pikel'naya et al. (2007); Irie et al. (2008); Wagner et al. (2011) where differences of 30% or less were observed. This 12% difference

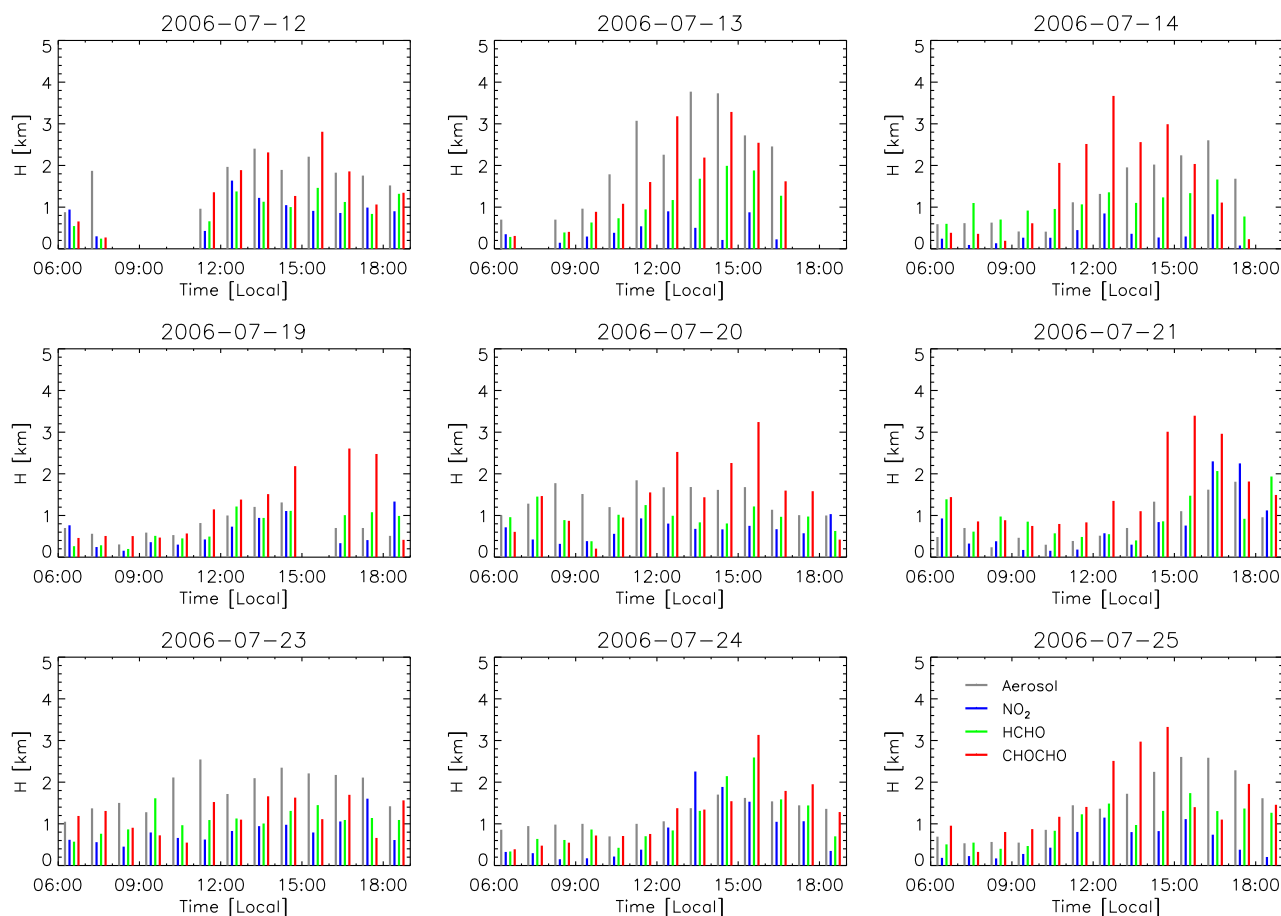


**Fig. 6.** Time series of mixing layer heights of  $\text{NO}_2$ , HCHO, CHOCHO and aerosol extinction (cf. Li et al., 2010) on the 9 cloud-free days during the PRIDE-PRD2006 campaign.

can be caused by two reasons, i.e. the inhomogeneous distribution of  $\text{NO}_2$ , and the uncertainty of parameters used in the RTM calculation. During the campaign, the  $\text{NO}_x$  emission usually occurred in the second half of the night or in the early morning. However, the relative difference of  $\text{NO}_2$  mixing ratios between the two techniques (i.e.  $\Delta\text{VCD}$ ) correlates neither with the time of the day ( $R^2=0$ ), nor with the  $\text{NO}_2$  layer height ( $R^2=0.01$ ), nor the wind speed ( $R^2=0.04$ ), suggesting the emission or transport effects, which can result in the inhomogeneity of  $\text{NO}_2$  distribution, have minor influence on the intercomparison results in this study. As discussed in Sect. 2.2, the aerosol properties, namely SSA,  $g$ , and AOD, are the major contributors to the systematic error of the MAX-DOAS  $\text{NO}_2$  retrieval. In the RTM calculation, SSA was fixed to the measured average value 0.85 and we assumed  $g$  to be constant at 0.68. However, due to the change of aerosol compositions and size distributions, the values of SSA and  $g$  change. Using the RTM we performed a number of sensitivity studies showing that an increase of SSA and  $g$  lead to higher values of modeled  $\text{NO}_2$  DSCDs and higher retrieved  $\text{NO}_2$  mixing ratios. Although the AOD

and the aerosol vertical distribution used in the RTM calculation were derived from the MAX-DOAS observations, they are sensitive to the values of SSA and  $g$  (Li et al., 2010). During the campaign, the uncertainty of SSA,  $g$ , and AOD were 10 %, 10 %, and 30 %, respectively, which can lead to an uncertainty of  $\approx 25$  % for the retrieved  $\text{NO}_2$  mixing ratios. In addition, the uncertainty of the RTM DSCDs simulation contributes another 10 % systematic error and the accuracy of the in-situ  $\text{NO}_2$  measurements was 13 %. Therefore, the 12 % difference between the  $\text{NO}_2$  mixing ratios observed by MAX-DOAS and by the in-situ technique are within the range provided by the systematic errors and the error of the slope.

The ground-based MAX-DOAS observations can also be used as an effective way for the validation of trace gas VCDs derived from satellite measurements, since both methods are based on the DOAS technique but differ in the viewing directions (i.e. one looking up to the sky, the other looking down to the earth). Here, we compared the tropospheric  $\text{NO}_2$  VCDs measured by MAX-DOAS and by OMI (Ozone Monitoring Instrument on board NASA's EOS-Aura satellite) for the BG

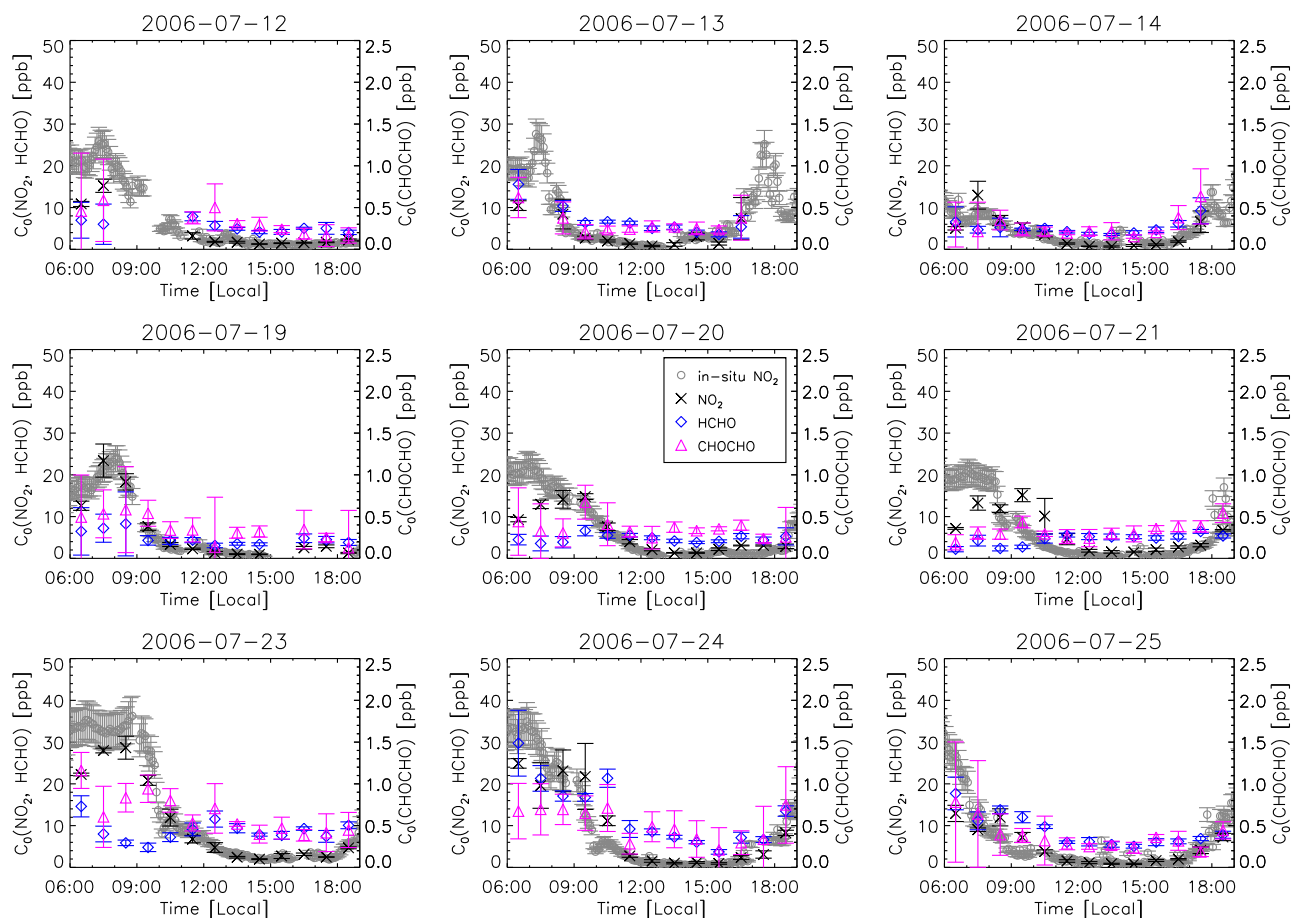


**Fig. 7.** Time series of  $\text{NO}_2$  (black cross), HCHO (blue diamond), and CHOCHO (pink triangle) mixing ratios near the ground surface derived from the MAX-DOAS measurements, and  $\text{NO}_2$  mixing ratios measured by in-situ chemiluminescence instrument (grey circle) on the 9 cloud-free days during the PRIDE-PRD2006 campaign.

site during the PRIDE-PRD2006 campaign. The OMI tropospheric vertical column densities of  $\text{NO}_2$  ( $\text{VCD}_{\text{omi}}$ ) were downloaded from <http://www.temis.nl> (DOMINO Version 2.0). The DOMINO products also include information on cloud fraction (CF). Details on the  $\text{NO}_2$   $\text{VCD}_{\text{omi}}$  and CF retrieval are described by Boersma et al. (2007) with recent updates in the DOMINO Product Specification Document ([http://www.temis.nl/docs/OMI\\_NO2\\_HE5\\_1.0.2.pdf](http://www.temis.nl/docs/OMI_NO2_HE5_1.0.2.pdf)). The uncertainties of  $\text{NO}_2$   $\text{VCD}_{\text{omi}}$  and CF are  $\approx 30\%$  and  $< 5\%$ , respectively, according to Boersma et al. (2007). Figure S5 shows the time series of  $\text{NO}_2$   $\text{VCD}_{\text{geo}}$ ,  $\text{VCD}_{\text{rtm}}$ , and  $\text{VCD}_{\text{omi}}$  during the entire campaign period. Given the ground pixel size of the OMI observation ( $\geq 340 \text{ km}^2$ ) and the satellite overpass time ( $\approx 14:00 \text{ LT}$ ) the cloud-free days discriminated from our sky-webcam images are only a subset of those by the OMI cloud fraction (i.e.  $\text{CF} \leq 0.5$ ). The relationship between MAX-DOAS and OMI measured tropospheric  $\text{NO}_2$  VCDs is shown in Fig. 9. The  $\text{NO}_2$   $\text{VCD}_{\text{omi}}$  were significantly lower than  $\text{NO}_2$   $\text{VCD}_{\text{geo}}$  when  $\text{CF} > 0.5$ , which can be expected since OMI only detects the  $\text{NO}_2$  absorption above

the cloud. When taking all measurement days into account, we found poor correlation ( $R^2 = 0.34$ ) of  $\text{VCD}_{\text{omi}}$  against  $\text{VCD}_{\text{geo}}$  (Fig. 9a). This is mainly caused by the large discrepancy between  $\text{VCD}_{\text{omi}}$  and  $\text{VCD}_{\text{geo}}$  in cloudy days. When we restrict to observations during the virtually cloud-free days,  $\text{VCD}_{\text{omi}}$  were found to correlate better with  $\text{VCD}_{\text{geo}}$  ( $R^2 = 0.71$ , Fig. 9a) and  $\text{VCD}_{\text{rtm}}$  ( $R^2 = 0.67$ , Fig. 9b). However,  $\text{VCD}_{\text{omi}}$  are on average 25% and 53% higher than  $\text{VCD}_{\text{geo}}$  and  $\text{VCD}_{\text{rtm}}$ , respectively. The majority of previous studies demonstrated that the tropospheric  $\text{NO}_2$  VCDs measured by OMI were between 10% and 50% lower than those measured by ground-based instruments, like MAX-DOAS and direct sun measurements (Brinksma et al., 2008; Celarier et al., 2008; Irie et al., 2008; Boersma et al., 2009). In contrast, Halla et al. (2011) observed at a rural site in Southwestern Ontario, that the  $\text{NO}_2$  VCDs measured by OMI can be 50% higher than those derived from MAX-DOAS measurements. Both, the overestimation and the underestimation were mainly attributed to the inhomogeneous distribution of  $\text{NO}_2$  especially for measurements in or near source regions,

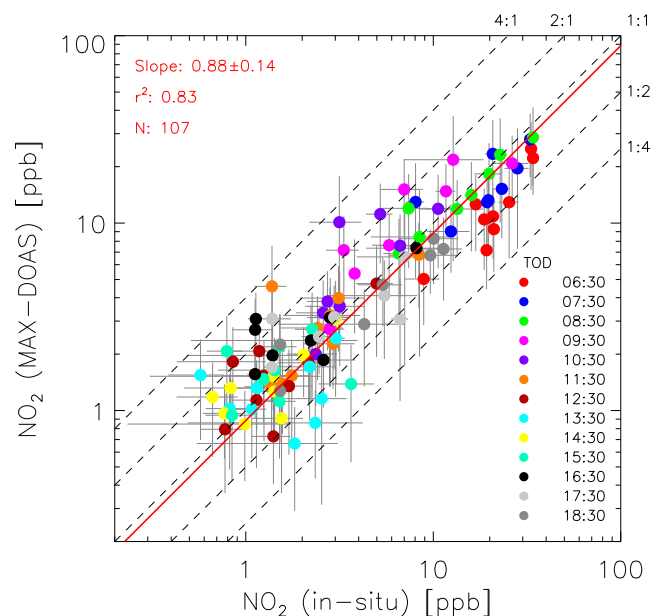


**Fig. 8.** Comparison of  $\text{NO}_2$  mixing ratios measured by MAX-DOAS and in-situ chemiluminescence technique during the PRIDE-PRD2006 campaign. Data displayed here are obtained on the 9 cloud-free days. The regression line is forced through the origin.

since OMI observations effectively average the  $\text{NO}_2$  concentrations over its field of view ( $\geq 340 \text{ km}^2$ ) while the ground-based instruments measure at a single spot.

The  $\text{NO}_2$  simulations of the CMAQ model were also compared to MAX-DOAS and in-situ measurement at the BG site during the cloud-free days. As shown in Figs. 3 and 10, the modeled  $\text{NO}_2$  concentrations follow the observations, but on average they are about 94 % higher than the observed values. The linear regression of  $\text{VCD}_{\text{CMAQ}}$  vs.  $\text{VCD}_{\text{ITM}}$  yielded a slope  $B_0 = 1.94 \pm 0.25$  while the surface layer  $\text{NO}_2$  concentrations of the CMAQ model and the in-situ instrument gave  $B_0 = 1.38 \pm 0.18$ . However, in the morning of 23 July and 24 July, the CMAQ modeled  $\text{NO}_2$  VCDs and surface layer concentrations are only 20–40 % of the measured values. This was caused by local emission events (i.e. biomass and electric cable burning) which are not included in the source inventory of the CMAQ model. The occurrence of the local emission events were identified by measurements of aerosol optical properties and OH reactivities at the BG site, as described by Garland et al. (2008) and Lou et al. (2010), respectively. After excluding the data in these periods, the modeled  $\text{NO}_2$  concentrations exceed the measured values by 150 % on average. In the CMAQ model, the simulated  $\text{NO}_2$  levels are mainly determined by the dilution effects and the  $\text{NO}_x$  emissions. The dilution effects are related with the wind speed and the vertical mixing. In the morning of 12 July and 19 July, when the modeled wind speeds were quite small and much lower than the local observations (Fig. S6), the accumulation of trace gases in the model can be expected and re-

sulted in the simulated  $\text{NO}_2$  concentrations being 5–8 times of the measured values. In other time periods, although the modeled wind speeds were either comparable with or higher than the locally measured values (Fig. S6), which is not in favor of the accumulation of air pollutants, the simulated  $\text{NO}_2$  concentrations are still  $\approx 65$  % higher than the measurement results.

When strong vertical mixing occurs,  $\text{NO}_2$  emitted or produced near the ground can be effectively transported to higher altitudes. The strength of the vertical mixing is reflected by the mixing layer height of  $\text{NO}_2$  ( $H_{\text{NO}_2}$ ). Figure 10 shows the time series of the  $\text{NO}_2$  concentrations modeled by CMAQ in different height ranges. In the early morning (before 07:00 LT) and late afternoon (after 17:00 LT), the modeled  $\text{NO}_2$  concentrations in the surface layer ( $c_{0 \rightarrow 18 \text{ m}}^{\text{NO}_2}$ ) were usually 5 times higher than those in the layer of 0–1 km ( $c_{0 \rightarrow 1 \text{ km}}^{\text{NO}_2}$ ), indicating that most of the  $\text{NO}_2$  was concentrated in a shallow layer above the ground and  $H_{\text{NO}_2}$  being less than 1 km. After 08:00 LT, the differences between  $c_{0 \rightarrow 18 \text{ m}}^{\text{NO}_2}$ ,  $c_{0 \rightarrow 1 \text{ km}}^{\text{NO}_2}$ , and  $c_{0 \rightarrow 3 \text{ km}}^{\text{NO}_2}$  became smaller, and  $c_{0 \rightarrow 1 \text{ km}}^{\text{NO}_2}$  nearly equals  $c_{0 \rightarrow 18 \text{ m}}^{\text{NO}_2}$ , suggesting an increase of  $H_{\text{NO}_2}$  to more than 1 km. The  $H_{\text{NO}_2}$  estimated from the modeled  $\text{NO}_2$  distributions were almost the same as those derived from the MAX-DOAS observations (cf.  $H_{\text{NO}_2}$  in Fig. 6). Since the CMAQ model can reproduce the observed  $H_{\text{NO}_2}$ , it is unlikely that the vertical mixing of  $\text{NO}_2$  in the model was underestimated. Given the discussion above, we conclude that the dilution effects can not explain the higher modeled  $\text{NO}_2$  concentrations than the measurements. In order to obtain better agreement between the modeled and measured  $\text{NO}_2$  concentrations reduced  $\text{NO}_x$  emissions in the source inventory of the CMAQ model seem to be necessary.

## 4.2 HCHO and CHOCHO

The HCHO and CHOCHO concentrations observed in this work are high for a rural site (cf. Table 4). This is consistent with PRD being identified as one of the hot spot regions of HCHO and CHOCHO by satellite measurements (De Smedt et al., 2008; Myriokefalitakis et al., 2008; Vrekoussis et al., 2009). Given HCHO and CHOCHO are mostly produced through the oxidation of different VOCs, their observed high concentrations indicate high levels of the precursor VOCs and the enormous  $\text{HO}_x$  turnover in the atmosphere of PRD region, which have also been demonstrated by Lou et al. (2010) and Lu et al. (2012). HCHO and CHOCHO at the BG site showed different diurnal variation than the observations in other places in the world (e.g., Munger et al., 1995; Lei et al., 2009), i.e. the maximum mixing ratios always occurred in early morning hours (Fig. 7) instead of around noon. The early occurrence of HCHO and CHOCHO peaks can be attributed to the oxidation of VOCs by OH radicals in the previous night. During the campaign, nighttime OH concentrations were constantly higher than zero and had an average of

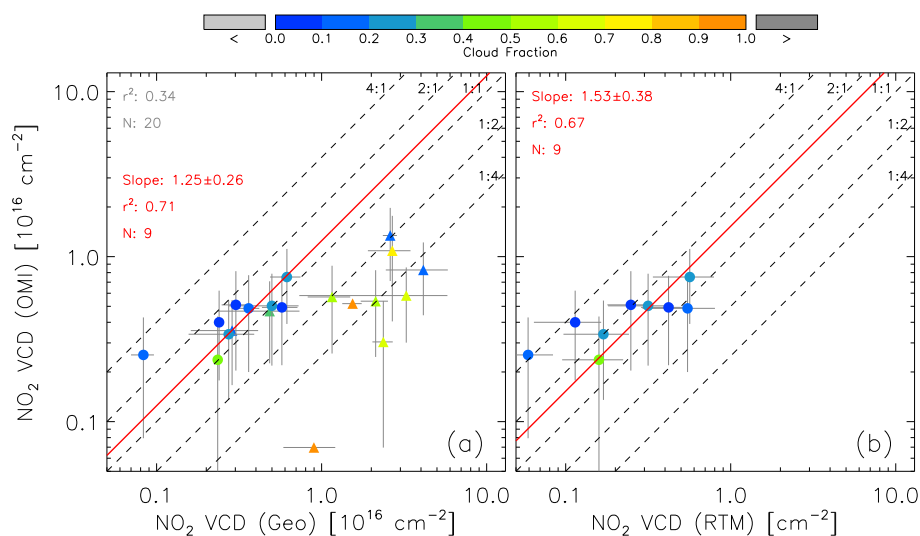


**Fig. 9.** Comparison of tropospheric  $\text{NO}_2$  VCDs derived from MAX-DOAS and OMI observations during the PRIDE-PRD2006 campaign. The x-axis in (a) and (b) corresponds to the  $\text{NO}_2$  VCDs derived from the geometric approach and the  $\text{NO}_2$  vertical distribution retrieval, respectively. The dots represent data obtained on the 9 cloud-free days. The regression and correlation results for the dots and triangles are shown in red and grey texts, respectively. The regression lines are forced through the origin.

**Table 4.** Overview of campaign average values of HCHO and CHOCHO mixing ratios (unit: ppb) and  $R_{\text{GF}}$  in different environments in the world. Results shown here are in conditions that simultaneous HCHO and CHOCHO measurements are available.

Location	Site	Period	HCHO	CHOCHO	$R_{\text{GF}}$	Reference
Caribbean Sea and Sargasso Sea	Marine	Autumn, Spring	0.4	0.08	0.200	Zhou and Mopper (1990)
Metter, Georgia, USA	Rural	Summer	3.6	0.02	0.006	Lee et al. (1995)
Pinnacles, Virginia, USA	Rural	Autumn	0.98	0.04	0.045	Munger et al. (1995)
San Nicolas, USA	Rural	Autumn	0.8	0.1	0.132	Grosjean et al. (1996)
Nashville, USA	Rural	Summer	4.2	0.07	0.017	Lee et al. (1998)
Giesta, Portugal	Rural	Summer	6.14	1.54	0.251	Borrego et al. (2000)
Pabsthum, Germany	Rural	Summer	2.58	0.03	0.012	Moortgat et al. (2002)
Anadia, Portugal	Rural	Summer	1.8	0.08	0.044	Cerqueira et al. (2003)
Goldlauter, Germany	Rural	Autumn	0.75	0.04	0.058	Müller et al. (2006)
Montelibretti, Italy	Rural	Summer	5.10	0.55	0.107	Possanzini et al. (2007)
		Autumn	3.38	0.22	0.064	
Sierra Nevada, USA	Rural	Autumn	6.88	0.03	0.004	Choi et al. (2010); Huisman et al. (2011)
Cabauw, Netherlands	Rural	Summer	2.5	0.08	0.036	Irie et al. (2011)
Sao Paulo, Barzil	Urban	Summer	10.4	0.7	0.092	Grosjean et al. (1990)
Los Angeles, USA	Urban	Summer	5.3	0.8	0.137	Grosjean et al. (1996)
		Autumn	1.0	0.3	0.300	Kawamura et al. (2000)
Las Vegas, USA	Urban	Summer	0.26	0.21	0.808	Jing et al. (2001)
		Winter	0.79	0.14	0.177	
Hongkong, China	Urban	–	11.3	1.5	0.122	Ho and Yu (2002)
Elizabeth, New Jersey, USA	Urban	Spring	5.29	0.72	0.136	Liu et al. (2006)
		Summer	3.86	0.71	0.183	
		Autumn	4.67	0.51	0.109	
		Winter	5.67	0.45	0.079	
Mexico City, Mexico	Urban	Spring	12.5	0.45	0.036	Lei et al. (2009)
Back Garden, China	Rural	Summer	7.0	0.4	0.062	This work

$\approx 1 \times 10^6 \text{ cm}^{-3}$  (Lu et al., 2012), while the average OH reactivities were  $30\text{--}50 \text{ s}^{-1}$  at night. Therefore, nighttime production of HCHO and CHOCHO is possible under these conditions. In the absence of photolysis, HCHO and CHOCHO

can easily accumulate. Moreover, the high HCHO concentrations in the early morning of 24, 25 July could also originate from direct emissions of the local combustion events. After sunrise, due to the increase of photolysis frequencies

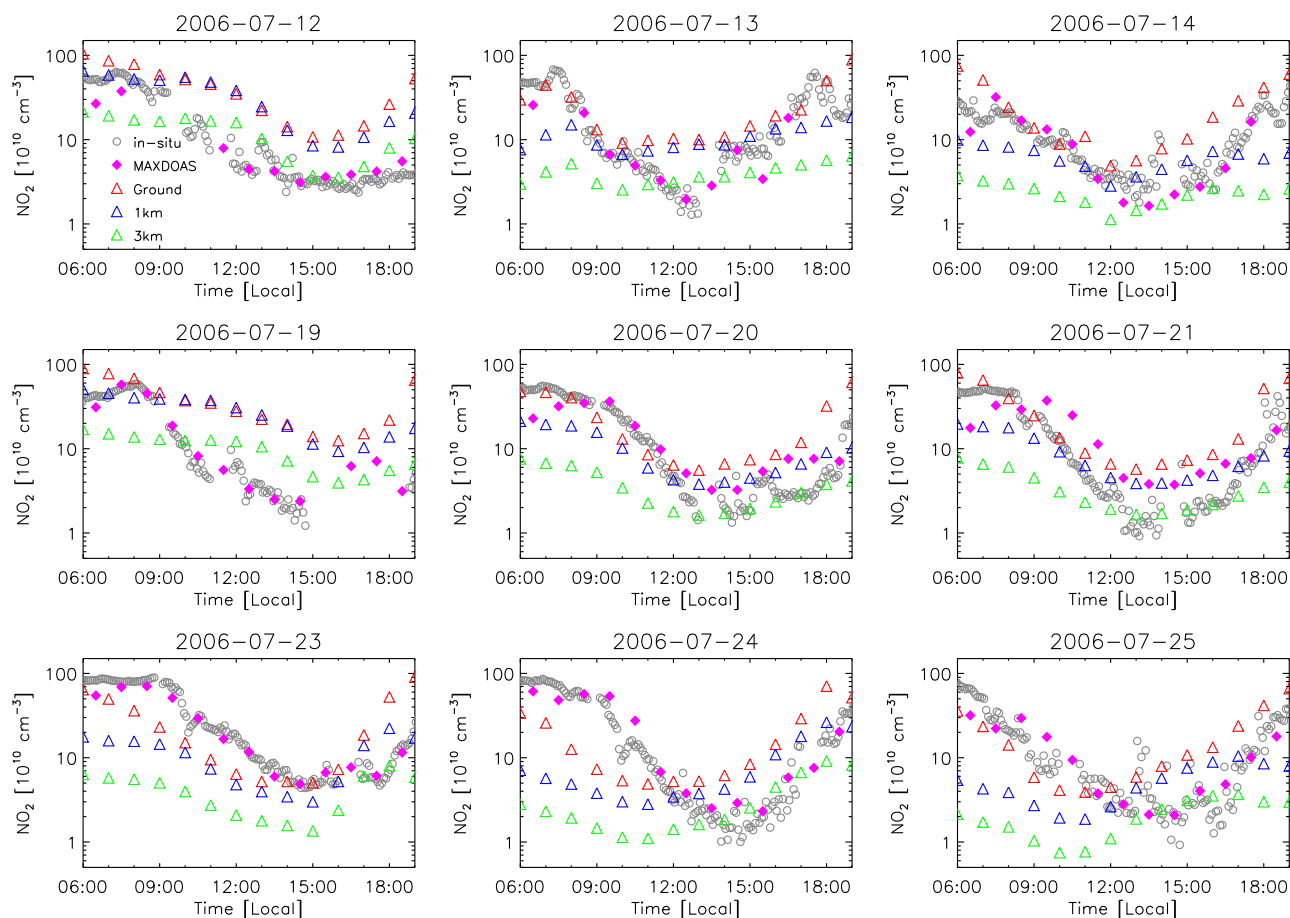


**Fig. 10.** Time series of  $\text{NO}_2$  concentrations measured by MAX-DOAS (full pink diamond) and in-situ chemiluminescence instrument (open grey circle), and simulated by the CMAQ model on the 9 cloud-free days during the PRIDE-PRD2006 campaign. The “ground” (open red triangle), “1 km” (blue triangle), and “3 km” (open green triangle) represent the average  $\text{NO}_2$  concentrations calculated by the CMAQ model in the layer of 0–18 m, 0–1 km, and 0–3 km, respectively.

and the mixing layer height, HCHO and CHOCHO mixing ratios started to decrease and became stable in the afternoon.

The mixing layer heights of CHOCHO ( $H_{\text{CHOCHO}}$ ) are higher than those of  $\text{NO}_2$  and HCHO especially in the afternoon (Fig. 6). Different trace gases have different mixing heights were also observed by Wagner et al. (2011) in summer time in Po Valley. The vertical distribution of a trace gas is determined by its production and destruction processes. During the campaign, the lifetimes of HCHO and CHOCHO around noon due to reaction with OH and photolysis were calculated to be  $\approx 1.4$  h and  $\approx 1.2$  h, respectively, based on the observed OH concentration of  $\approx 1.4 \times 10^7 \text{ cm}^{-3}$  and the measured photolysis frequency of  $\approx 6 \times 10^{-5} \text{ s}^{-1}$  for HCHO and  $\approx 9 \times 10^{-5} \text{ s}^{-1}$  for CHOCHO. The lifetime of  $\text{NO}_2$ , which is mainly defined by the OH +  $\text{NO}_2$  reaction during daytime, was around 30 min. Due to the short lifetime of  $\text{NO}_2$ , lower  $H_{\text{NO}_2}$  than  $H_{\text{CHOCHO}}$  can be expected. Although the lifetime of HCHO and CHOCHO were comparable, the production pathways of HCHO and CHOCHO can

be different. First, compared to CHOCHO, HCHO has possibly primary sources. A continuous surface source of HCHO can result in the detected HCHO layer much lower than the CHOCHO layer. However, at the BG site there was no evidence that direct emission of HCHO was occurring during daytime. Second, our recent model studies suggest that the degradation of isoprene was the major pathway producing HCHO and CHOCHO in the afternoon at the BG site; its contribution to the HCHO and CHOCHO production was around 50%. While the other half of HCHO production was caused by the oxidation of alkenes, degradation of aromatics accounted for the other half of CHOCHO production (Li et al., 2013). For isoprene oxidation we found from our model study that most HCHO was formed as the first generation product whereas CHOCHO was mostly produced in the third and fourth generation of the isoprene oxidation. At the BG site, the noontime OH concentration of  $1.4 \times 10^7 \text{ cm}^{-3}$  resulted in a lifetime of isoprene of around 10 min. This is shorter than the typical mixing time in the boundary layer of

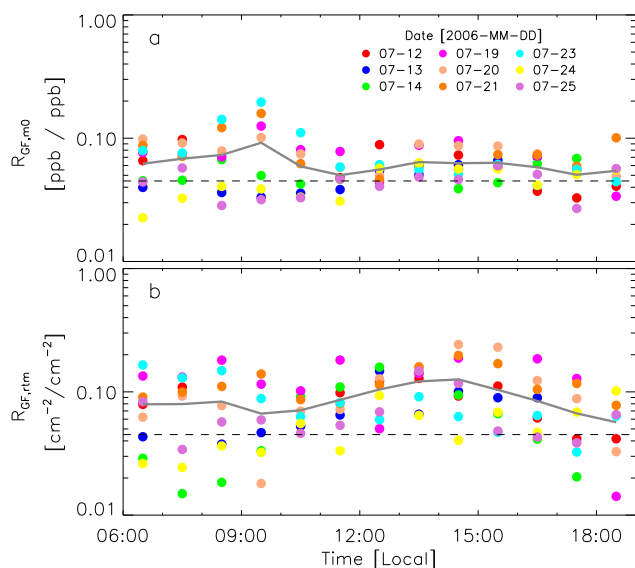


**Fig. 11.** Diurnal variation of CHOCHO/HCHO ratio ( $R_{GF}$ ) on the 9 cloud-free days during the PRIDE-PRD2006 campaign. The dots are values calculated from individually measured  $m_0$  (panel a) and  $VCD_{rtm}$  (panel b). Solid lines refer to the average values of the individual points.

$\approx 15$  min (c.f. Stull, 1988). When isoprene is degraded the HCHO production occurs earlier, i.e. at lower altitudes, than the CHOCHO production. Moreover, due to the faster reaction rate with OH, the lifetimes of isoprene and alkenes are shorter than those of aromatics, which can result in different vertical distribution between different NMHCs. According to the CMAQ model simulation, aromatics were mixed to higher altitudes (up to 4 km) than isoprene and alkenes at BG site, especially around noon (Fig. S7). Since aromatics are the other group of CHOCHO precursor of besides isoprene, production of CHOCHO at higher altitudes can be expected.

Both species, CHOCHO and HCHO, are mainly produced through hydrocarbon oxidation. The ratio of CHOCHO to HCHO ( $R_{GF}$ ) was used in a number of studies to identify the sources of VOCs since CHOCHO and HCHO have different precursors or different formation pathways (e.g., Vrekoussis et al., 2010). Figure 11 shows the diurnal variation of the CHOCHO to HCHO ratio ( $R_{GF}$ ) in the 9 cloud-free days.  $R_{GF}$  calculated from the mixing ratio near the ground surface ( $R_{GF,m0}$ ) have similar average value as that from  $VCD_{rtm}$  ( $R_{GF,m0} = 0.062 \pm 0.027$ ,  $R_{GF,rtm} = 0.088 \pm 0.049$ ). In general, both  $R_{GF,m0}$  and  $R_{GF,rtm}$  do not show prominent diurnal variations. However, in the early morning of 24 and 25 July, when strong combustion events existed in surrounding areas,  $R_{GF}$  were significantly lower than in other periods. In addition, the geometric approach for HCHO and CHOCHO showed deviations from retrieval using the radiative transfer (Figs. S3 and S4). It also tends to overestimated the HCHO and CHOCHO VCDs. Therefore, the correlation between

$R_{GF,geo}$  (i.e.  $R_{GF}$  calculated from  $VCD_{geo}$ ) and  $R_{GF,rtm}$  is only modest ( $R^2 = 0.39$ ).

$R_{GF}$  depends on many factors including primary emissions, compositions and concentrations of precursor VOCs, and OH concentrations.  $R_{GF}$  higher than 0.5 were found by Schauer et al. (2001) in biomass burning emissions, whilst  $R_{GF}$  were in the range of 0.02–0.09 in vehicle exhausts (Schauer et al., 1999, 2002). Since different types of VOCs (i.e. alkanes, alkenes, aromatics, oxygenated VOCs) have different yields of HCHO and CHOCHO, values of  $R_{GF}$  can be different when the VOCs compositions change. Table 4 lists  $R_{GF}$  obtained in different environments around the world. In general,  $R_{GF}$  in rural areas are below 0.1, whilst values higher than 0.1 exist in urban areas. Besides the lower concentrations of ambient VOCs, most rural areas are strongly influenced by biogenic VOC emissions, e.g. isoprene, terpenes, and 2-methyl-3-butene-2-ol (MBO) (Lee et al., 1995; Munger et al., 1995; Huisman et al., 2011). Compared to anthropogenic VOCs (e.g. aromatics), the CHOCHO yield from isoprene or terpenes oxidations are much lower (Fu et al., 2008). Therefore, increase of  $R_{GF}$  can be expected when the VOCs composition is changing from isoprene dominated to aromatics dominated. For example, Giesta, Portugal is located in a rural area, however, the strong influence of anthropogenic emissions from industries in surrounding areas cause high levels of HCHO, CHOCHO, and  $R_{GF}$ . On the other hand, given primary emission (e.g. traffic) can account for a large fraction of ambient HCHO but barely contributes to CHOCHO (Grosjean et al., 1990; Lei et al., 2009), the prevailing anthropogenic sources can also cause a decrease of  $R_{GF}$ . This is the case that low  $R_{GF}$  was observed in urban areas like Sao Paulo, Brazil and Mexico City, Mexico. It was also found that, for the same measurement site (i.e. Montelibretti, Italy, Las Vegas, USA, and Elizabeth, USA),  $R_{GF}$  obtained in summer are higher than in other seasons (Jing et al., 2001; Liu et al., 2006; Possanzini et al., 2007). This is because summer time is usually accompanied by high solar radiation, temperature, and humidity, which are in favor of the photochemical reactions producing HCHO, CHOCHO, and other secondary products.  $R_{GF}$  obtained at the BG site are higher than the values in most rural areas but close to those in urban conditions. As described by Lu et al. (2012), during the PRIDE-PRD2006 campaign, the detected air masses were mixtures of anthropogenic and biogenic emissions. Additionally, the observed high OH and  $k_{OH}$  level indicate the fast ongoing photochemistry which has rarely been reported for other places in the world. However, in the relationship between  $R_{GF}$  and other measured parameters (e.g.  $NO_x$ ,  $O_3$ , VOCs, OH,  $k_{OH}$ ,  $OH \times k_{OH}$ ), no correlations were found. This is probably due to  $R_{GF}$  is determined by the combination of several factors (e.g. the concentration and composition of precursors, the OH level, the photolysis frequencies, etc), which is difficult to be reflected by a single parameter.

The spatial distribution of  $R_{GF}$  and its implication on VOC source types have been investigated by Vrekoussis et al. (2010) using satellite measurements. Their observed  $R_{GF}$  of  $\approx 0.04$  for Southern Asia is lower than the values obtained at the BG site. This difference can be explained by the different spatial resolution between the satellite and local measurements. Vrekoussis et al. (2010) suggest that  $R_{GF}$  in the range of 0.04–0.06 can represent regions where biogenic emissions are the dominant primary VOC sources, while values lower than 0.04 indicate elevated anthropogenic VOC emissions. However, referring to Table 4, their suggestion seems only consistent with the observations for rural areas. The major argument of  $R_{GF} < 0.04$  representing regions influenced by anthropogenic emissions is, the primary HCHO from anthropogenic sources can cause a decrease of  $R_{GF}$  (Vrekoussis et al., 2010). As discussed above, this is indeed the case for Mexico City, Mexico, but might not always be true for areas where the primary HCHO concentration is low but anthropogenic VOCs (e.g. aromatics) are at high level. According to Table 4,  $R_{GF}$  in urban areas are in general higher than 0.04 by a factor of 2. To solve the difference between the conclusion of Vrekoussis et al. (2010) and this study, more simultaneous HCHO and CHOCHO measurements at different locations and seasons are needed. Furthermore, it is necessary to apply the photochemical modeling of HCHO and CHOCHO in terms of VOC compositions.

## 5 Summary and conclusion

During the PRIDE-PRD2006 campaign in Southern China in July 2006, we performed MAX-DOAS measurements for  $\text{NO}_2$ , HCHO, and CHOCHO at a rural site 60 km NW of downtown Guangzhou. Under the assumption of a “box profile” setup for the three trace gases, their tropospheric vertical column densities, mixing layer heights, and mixing ratios at the ground have been retrieved by an automated algorithm.

- The simple geometric approach is able to provide good estimates of the  $\text{NO}_2$  tropospheric VCDs even under the relatively high aerosol loads ( $\text{AOD} = 1.56 \pm 0.97$ ) encountered here.
- Tropospheric  $\text{NO}_2$  VCDs observed by OMI were found to be 50% higher than by our ground-based MAX-DOAS measurements, which can be due to the inhomogeneous  $\text{NO}_2$  distribution in PRD.
- A comparison to the 3-D chemical transport model CMAQ showed a high degree of correlation for  $\text{NO}_2$  VCDs and  $\text{NO}_2$  ground level concentrations but the model overestimates the measured values indicating a need for a reduction of the  $\text{NO}_x$  emission strength in the source inventory.
- The HCHO and CHOCHO concentrations and their ratios  $R_{GF}$  were higher than expected from previous stud-

ies. This can be attributed to the high photochemical turnover in the PRD region.

- Different from satellite observations, our ground-based measurements indicate that  $R_{GF}$  are lower than 0.1 in rural areas but increase with higher anthropogenic emissions.

Based on these findings, simultaneous measurements of HCHO and CHOCHO and their precursors as well as photochemical modeling are necessary in order to obtain a clearer picture on the influence of anthropogenic and biogenic emissions on  $R_{GF}$ . We also showed in this case study for  $\text{NO}_2$  that MAX-DOAS can serve as an useful tool for 3-d CTM evaluation and for satellite validation even under specific conditions here. The automated MAX-DOAS retrieval of VCDs and mixing layer heights are a first step towards using MAX-DOAS product for data assimilation forecast models.

**Supplementary material related to this article is available online at:** <http://www.atmos-chem-phys.net/13/2133/2013/acp-13-2133-2013-supplement.pdf>.

*Acknowledgements.* The authors like to thank Roman Sinreich, Udo Frieb, and Ulrich Platt (Heidelberg) for the lending of the Mini-MAX DOAS instrument, the MiniMax software, and fruitful discussions. The technical help and support at the field site from the PRIDE-PRD2006 campaign team, especially Rolf Häsel (Jülich), Min Hu, Limin Zeng, and Yuanhang Zhang (Beijing) are gratefully acknowledged. We thank all participants of the distributed computing of the RTM. We acknowledge the free use of tropospheric  $\text{NO}_2$  column data from the OMI sensor from [www.temis.nl](http://www.temis.nl). This work was supported by the China National Basic Research and Development Program 2002CB410801, and the National High Technology Research and Development Program of China (863 Program) 2006AA06A301.

The service charges for this open access publication have been covered by a Research Centre of the Helmholtz Association.

Edited by: S. C. Liu

## References

- Bobrowski, N., Honninger, G., Galle, B., and Platt, U.: Detection of bromine monoxide in a volcanic plume, *Nature*, 423, 273–276, doi:10.1038/nature01625, 2003.
- Boersma, K. F., Eskes, H. J., Veefkind, J. P., Brinksma, E. J., van der A, R. J., Sneep, M., van den Oord, G. H. J., Levelt, P. F., Stammes, P., Gleason, J. F., and Bucela, E. J.: Near-real time retrieval of tropospheric  $\text{NO}_2$  from OMI, *Atmos. Chem. Phys.*, 7, 2103–2118, doi:10.5194/acp-7-2103-2007, 2007.
- Boersma, K. F., Jacob, D. J., Trainic, M., Rudich, Y., DeSmedt, I., Dirksen, R., and Eskes, H. J.: Validation of urban  $\text{NO}_2$  concentrations and their diurnal and seasonal variations observed from

- the SCIAMACHY and OMI sensors using in situ surface measurements in Israeli cities, *Atmos. Chem. Phys.*, 9, 3867–3879, doi:10.5194/acp-9-3867-2009, 2009.
- Borrego, C., Gomes, P., Barros, N., and Miranda, A. I.: Importance of handling organic atmospheric pollutants for assessing air quality, *J. Chromatogr. A*, 889, 271–279, doi:10.1016/S0021-9673(00)00230-2, 2000.
- Brinksmas, E. J., Pinardi, G., Volten, H., Braak, R., Richter, A., Schöhardt, A., van Roozendaal, M., Fayt, C., Hermans, C., Dirksen, R. J., Vlemmix, T., Berkhout, A. J. C., Swart, D. P. J., Oetjen, H., Wittrock, F., Wagner, T., Ibrahim, O. W., de Leeuw, G., Moerman, M., Curier, R. L., Celarier, E. A., Cede, A., Knap, W. H., Veefkind, J. P., Eskes, H. J., Allaart, M., Rothe, R., PETERS, A. J. M., and Levelt, P. F.: The 2005 and 2006 DANDELIONS NO<sub>2</sub> and aerosol intercomparison campaigns, *J. Geophys. Res.*, 113, D16S46, doi:10.1029/2007JD008808, 2008.
- Bussemer, M.: Der Ring-Effekt: Ursachen und Einfluß auf die spektroskopische Messung stratosphäischer Spurenstoffe, Diploma thesis, Universität Heidelberg, Heidelberg, Germany, 1993.
- Celarier, E. A., Brinksmas, E. J., Gleason, J. F., Veefkind, J. P., Cede, A., Herman, J. R., Ionov, D., Goutail, F., Pommereau, J.-P., Lambert, J.-C., van Roozendaal, M., Pinardi, G., Wittrock, F., Schöhardt, A., Richter, A., Ibrahim, O. W., Wagner, T., Borkov, B., Mount, G., Spinei, E., Chen, C. M., Pongetti, T. J., Sander, S. P., Bucseala, E. J., Wenig, M. O., Swart, D. P. J., Volten, H., Kroon, M., and Levelt, P. F.: Validation of Ozone Monitoring Instrument nitrogen dioxide columns, *J. Geophys. Res.*, 113, D15S15, doi:10.1029/2007JD008908, 2008.
- Cerqueira, M. A., Pio, C. A., Gomes, P. A., Matos, J. S., and Nunes, T. V.: Volatile organic compounds in rural atmospheres of Central Portugal, *Sci. Total Environ.*, 313, 49–60, doi:10.1016/S0048-9697(03)00250-X, 2003.
- Choi, W., Faloona, I. C., Bouvier-Brown, N. C., McKay, M., Goldstein, A. H., Mao, J., Brune, W. H., LaFranchi, B. W., Cohen, R. C., Wolfe, G. M., Thornton, J. A., Sonnenfroh, D. M., and Millet, D. B.: Observations of elevated formaldehyde over a forest canopy suggest missing sources from rapid oxidation of arboreal hydrocarbons, *Atmos. Chem. Phys.*, 10, 8761–8781, doi:10.5194/acp-10-8761-2010, 2010.
- De Smedt, I., Müller, J.-F., Stavrou, T., van der A, R., Eskes, H., and Van Roozendaal, M.: Twelve years of global observations of formaldehyde in the troposphere using GOME and SCIAMACHY sensors, *Atmos. Chem. Phys.*, 8, 4947–4963, doi:10.5194/acp-8-4947-2008, 2008.
- Deutschmann, T., Beirle, S., Frieß, U., Grzegorski, M., Kern, C., Kritzen, L., Platt, U., Prados-Román, C., Pukite, J., Wagner, T., Werner, B., and Pfeilsticker, K.: The Monte Carlo atmospheric radiative transfer model McArtim: introduction and validation of Jacobians and 3D features, *J. Quant. Spectrosc. Ra.*, 112, 1119–1137, doi:10.1016/j.jqsrt.2010.12.009, 2011.
- Fan, S. J., Fan, Q., Yu, W., Luo, X. Y., Wang, B. M., Song, L. L., and Leong, K. L.: Atmospheric boundary layer characteristics over the Pearl River Delta, China, during the summer of 2006: measurement and model results, *Atmos. Chem. Phys.*, 11, 6297–6310, doi:10.5194/acp-11-6297-2011, 2011.
- Fried, A., Crawford, J., Olson, J., Walega, J., Potter, W., Wert, B., Jordan, C., Anderson, B., Shetter, R., Lefer, B., Blake, D., Blake, N., Meinardi, S., Heikes, B., O'Sullivan, D., Snow, J., Fuelberg, H., Kiley, C. M., Sandholm, S., Tan, D., Sachse, G., Singh, H., Faloona, I., Harward, C. N., and Carmichael, G. R.: Airborne tunable diode laser measurements of formaldehyde during TRACE-P: distributions and box model comparisons, *J. Geophys. Res.*, 108, 8798, doi:10.1029/2003jd003451, 2003.
- Fu, T.-M., Jacob, D. J., Wittrock, F., Burrows, J. P., Vrekoussis, M., and Henze, D. K.: Global budgets of atmospheric glyoxal and methylglyoxal, and implications for formation of secondary organic aerosols, *J. Geophys. Res.*, 113, D15303, doi:10.1029/2007JD009505, 2008.
- Garland, R. M., Yang, H., Schmid, O., Rose, D., Nowak, A., Achtert, P., Wiedensohler, A., Takegawa, N., Kita, K., Miyazaki, Y., Kondo, Y., Hu, M., Shao, M., Zeng, L. M., Zhang, Y. H., Andreae, M. O., and Pöschl, U.: Aerosol optical properties in a rural environment near the mega-city Guangzhou, China: implications for regional air pollution, radiative forcing and remote sensing, *Atmos. Chem. Phys.*, 8, 5161–5186, doi:10.5194/acp-8-5161-2008, 2008.
- Greenblatt, G. D., Orlando, J. J., Burkholder, J. B., and Ravishankara, A. R.: Absorption measurements of oxygen between 330 and 1140 nm, *J. Geophys. Res.*, 95, 18577–18582, doi:10.1029/JD095iD11p18577, 1990.
- Grosjean, D., Miguel, A. H., and Tavares, T. M.: Urban air pollution in Brazil: acetaldehyde and other carbonyls, *Atmos. Environ. B-Urb.*, 24, 101–106, doi:10.1016/0957-1272(90)90015-M, 1990.
- Grosjean, E., Grosjean, D., Fraser, M. P., and Cass, G. R.: Air quality model evaluation data for organics. 2. C<sub>1</sub>-C<sub>14</sub> carbonyls in Los Angeles air, *Environ. Sci. Technol.*, 30, 2687, doi:10.1021/es950758w, 1996.
- Halla, J. D., Wagner, T., Beirle, S., Brook, J. R., Hayden, K. L., O'Brien, J. M., Ng, A., Majonis, D., Wenig, M. O., and McLaren, R.: Determination of tropospheric vertical columns of NO<sub>2</sub> and aerosol optical properties in a rural setting using MAX-DOAS, *Atmos. Chem. Phys.*, 11, 12475–12498, doi:10.5194/acp-11-12475-2011, 2011.
- Heckel, A., Richter, A., Tarsu, T., Wittrock, F., Hak, C., Pundt, I., Junkermann, W., and Burrows, J. P.: MAX-DOAS measurements of formaldehyde in the Po-Valley, *Atmos. Chem. Phys.*, 5, 909–918, doi:10.5194/acp-5-909-2005, 2005.
- Hendrick, F., Van Roozendaal, M., Kylling, A., Petritoli, A., Rozanov, A., Sanghavi, S., Schofield, R., von Friedeburg, C., Wagner, T., Wittrock, F., Fonteyn, D., and De Mazière, M.: Intercomparison exercise between different radiative transfer models used for the interpretation of ground-based zenith-sky and multi-axis DOAS observations, *Atmos. Chem. Phys.*, 6, 93–108, doi:10.5194/acp-6-93-2006, 2006.
- Ho, S. S. H. and Yu, J. Z.: Feasibility of collection and analysis of airborne carbonyls by on-sorbent derivatization and thermal desorption, *Anal. Chem.*, 74, 1232–1240, doi:10.1021/ac015708q, 2002.
- Hofzumahaus, A., Rohrer, F., Lu, K., Bohn, B., Brauers, T., Chang, C.-C., Fuchs, H., Holland, F., Kita, K., Kondo, Y., Li, X., Lou, S., Shao, M., Zeng, L., Wahner, A., and Zhang, Y.: Amplified trace gas removal in the troposphere, *Science*, 324, 1702–1704, doi:10.1126/science.1164566, 2009.
- Hönninger, G. and Platt, U.: Observations of BrO and its vertical distribution during surface ozone depletion at Alert, *Atmos. Environ.*, 36, 2481–2489, doi:10.1016/S1352-2310(02)00104-8, 2002.

- Hua, W., Chen, Z. M., Jie, C. Y., Kondo, Y., Hofzumahaus, A., Takegawa, N., Chang, C. C., Lu, K. D., Miyazaki, Y., Kita, K., Wang, H. L., Zhang, Y. H., and Hu, M.: Atmospheric hydrogen peroxide and organic hydroperoxides during PRIDE-PRD'06, China: their concentration, formation mechanism and contribution to secondary aerosols, *Atmos. Chem. Phys.*, 8, 6755–6773, doi:10.5194/acp-8-6755-2008, 2008.
- Huisman, A. J., Hottle, J. R., Galloway, M. M., DiGangi, J. P., Coens, K. L., Choi, W., Faloona, I. C., Gilman, J. B., Kuster, W. C., de Gouw, J., Bouvier-Brown, N. C., Goldstein, A. H., LaFranchi, B. W., Cohen, R. C., Wolfe, G. M., Thornton, J. A., Docherty, K. S., Farmer, D. K., Cubison, M. J., Jimenez, J. L., Mao, J., Brune, W. H., and Keutsch, F. N.: Photochemical modeling of glyoxal at a rural site: observations and analysis from BEARPEX 2007, *Atmos. Chem. Phys.*, 11, 8883–8897, doi:10.5194/acp-11-8883-2011, 2011.
- Inomata, S., Tanimoto, H., Kameyama, S., Tsunogai, U., Irie, H., Kanaya, Y., and Wang, Z.: Technical Note: Determination of formaldehyde mixing ratios in air with PTR-MS: laboratory experiments and field measurements, *Atmos. Chem. Phys.*, 8, 273–284, doi:10.5194/acp-8-273-2008, 2008.
- Irie, H., Kanaya, Y., Akimoto, H., Tanimoto, H., Wang, Z., Gleason, J. F., and Bucsel, E. J.: Validation of OMI tropospheric NO<sub>2</sub> column data using MAX-DOAS measurements deep inside the North China Plain in June 2006: Mount Tai Experiment 2006, *Atmos. Chem. Phys.*, 8, 6577–6586, doi:10.5194/acp-8-6577-2008, 2008.
- Irie, H., Takashima, H., Kanaya, Y., Boersma, K. F., Gast, L., Wittrock, F., Brunner, D., Zhou, Y., and Van Roozendaal, M.: Eight-component retrievals from ground-based MAX-DOAS observations, *Atmos. Meas. Tech.*, 4, 1027–1044, doi:10.5194/amt-4-1027-2011, 2011.
- Jing, L. H., Steinberg, S. M., and Johnson, B. J.: Aldehyde and monocyclic aromatic hydrocarbon mixing ratios at an urban site in Las Vegas, Nevada, *J. Air Waste Manage.*, 51, 1359–1366, 2001.
- Junkermann, W.: On the distribution of formaldehyde in the western Po-Valley, Italy, during FORMAT 2002/2003, *Atmos. Chem. Phys.*, 9, 9187–9196, doi:10.5194/acp-9-9187-2009, 2009.
- Kawamura, K., Steinberg, S., and Kaplan, I. R.: Homologous series of C<sub>1</sub>–C<sub>10</sub> monocarboxylic acids and C<sub>1</sub>–C<sub>6</sub> carbonyls in Los Angeles air and motor vehicle exhausts, *Atmos. Environ.*, 34, 4175–4191, 2000.
- Klippel, T., Fischer, H., Bozem, H., Lawrence, M. G., Butler, T., Jöckel, P., Tost, H., Martinez, M., Harder, H., Regelin, E., Sander, R., Schiller, C. L., Stickler, A., and Lelieveld, J.: Distribution of hydrogen peroxide and formaldehyde over Central Europe during the HOOVER project, *Atmos. Chem. Phys.*, 11, 4391–4410, doi:10.5194/acp-11-4391-2011, 2011.
- Kurucz, R. L., Furenlid, I. J., and Testerman, L.: Solar Flux Atlas from 296 to 1300 nm, Technical report, National Solar Observatory, 1984.
- Lee, Y.-N., Zhou, X., and Hallock, K.: Atmospheric carbonyl compounds at a rural Southeastern United States site, *J. Geophys. Res.*, 100, 25933–25944, doi:10.1029/95jd02605, 1995.
- Lee, Y. N., Zhou, X., Kleinman, L. I., Nunnermacker, L. J., Springston, S. R., Daum, P. H., Newman, L., Keigley, W. G., Holdren, M. W., Spicer, C. W., Young, V., Fu, B., Parrish, D. D., Holloway, J., Williams, J., Roberts, J. M., Ryerson, T. B., and Fehsenfeld, F. C.: Atmospheric chemistry and distribution of formaldehyde and several multioxygenated carbonyl compounds during the 1995 Nashville/Middle Tennessee Ozone Study, *J. Geophys. Res.*, 103, 22449–22462, doi:10.1029/98jd01251, 1998.
- Lei, W., Zavala, M., de Foy, B., Volkamer, R., Molina, M. J., and Molina, L. T.: Impact of primary formaldehyde on air pollution in the Mexico City Metropolitan Area, *Atmos. Chem. Phys.*, 9, 2607–2618, doi:10.5194/acp-9-2607-2009, 2009.
- Leser, H., Hönninger, G., and Platt, U.: MAX-DOAS measurements of BrO and NO<sub>2</sub> in the marine boundary layer, *Geophys. Res. Lett.*, 30, 1537, doi:10.1029/2002gl015811, 2003.
- Li, X., Brauers, T., Shao, M., Garland, R. M., Wagner, T., Deutschmann, T., and Wahner, A.: MAX-DOAS measurements in southern China: retrieval of aerosol extinctions and validation using ground-based in-situ data, *Atmos. Chem. Phys.*, 10, 2079–2089, doi:10.5194/acp-10-2079-2010, 2010.
- Li, X., Brauers, T., Häseler, R., Bohn, B., Hofzumahaus, A., Holland, F., Lu, K. D., Rohrer, F., Hu, M., Zeng, L. M., Zhang, Y. H., Garland, R., Su, H., Nowak, A., Takegawa, N., Shao, M., and Wahner, A.: Exploring the atmospheric chemistry of nitrous acid (HONO) at a rural site in Southern China, *Atmos. Chem. Phys. Discuss.*, 11, 27591–27635, doi:10.5194/acpd-11-27591-2011, 2011.
- Li, X., Brauers, T., Hofzumahaus, A., Lu, K., Li, Y. P., Shao, M., Wagner, T., and Wahner, A.: MAX-DOAS measurements of NO<sub>2</sub>, HCHO and CHOCHO at a rural site in Southern China, *Atmos. Chem. Phys. Discuss.*, 12, 3983–4029, doi:10.5194/acpd-12-3983-2012, 2012.
- Li, X., Brauers, T., Rohrer, F., Shao, M., Lu, K., Bohn, B., Fuchs, H., Hofzumahaus, A., Holland, F., Hu, M., Lou, S., Nowak, A., Takegawa, N., Zeng, L. M., Zhang, Y. H., and Wahner, A.: Modeling of HCHO and CHOCHO at a rural site in southern China during PRIDE-PRD2006 campaign, *Atmos. Chem. Phys. Discuss.*, under preparation, 2013.
- Liu, W., Zhang, J., Kwon, J., Weisel, C., Turpin, B., Zhang, L., Korn, L., Morandi, M., Stock, T., and Colome, S.: Concentrations and source characteristics of airborne carbonyl compounds measured outside urban residences, *J. Air Waste Manage.*, 56, 1196–1204, 2006.
- Lou, S., Holland, F., Rohrer, F., Lu, K., Bohn, B., Brauers, T., Chang, C. C., Fuchs, H., Häseler, R., Kita, K., Kondo, Y., Li, X., Shao, M., Zeng, L., Wahner, A., Zhang, Y., Wang, W., and Hofzumahaus, A.: Atmospheric OH reactivities in the Pearl River Delta – China in summer 2006: measurement and model results, *Atmos. Chem. Phys.*, 10, 11243–11260, doi:10.5194/acp-10-11243-2010, 2010.
- Lu, K. D., Rohrer, F., Holland, F., Fuchs, H., Bohn, B., Brauers, T., Chang, C. C., Häseler, R., Hu, M., Kita, K., Kondo, Y., Li, X., Lou, S. R., Nehr, S., Shao, M., Zeng, L. M., Wahner, A., Zhang, Y. H., and Hofzumahaus, A.: Observation and modelling of OH and HO<sub>2</sub> concentrations in the Pearl River Delta 2006: a missing OH source in a VOC rich atmosphere, *Atmos. Chem. Phys.*, 12, 1541–1569, doi:10.5194/acp-12-1541-2012, 2012.
- Meller, R. and Moortgat, G. K.: Temperature dependence of the absorption cross sections of formaldehyde between 223 and 323 K in the wavelength range 225–375 nm, *J. Geophys. Res.*, 105, 7089–7101, doi:10.1029/1999jd901074, 2000.

- Moortgat, G. K., Grossmann, D., Boddenberg, A., Dallmann, G., Ligon, A. P., Turner, W. V., Gäb, S., Slemr, F., Wieprecht, W., Acker, K., Kibler, M., Schlomski, S., and Bächmann, K.: Hydrogen peroxide, organic peroxides and higher carbonyl compounds determined during the BERLIOZ campaign, *J. Atmos. Chem.*, 42, 443–463, doi:10.1023/A:1015743013107, 2002.
- Müller, K., Haferkorn, S., Grabmer, W., Wisthaler, A., Hansel, A., Kreuzwieser, J., Cojocariu, C., Rennenberg, H., and Herrmann, H.: Biogenic carbonyl compounds within and above a coniferous forest in Germany, *Atmos. Environ.*, 40, 81–91, doi:10.1016/j.atmosenv.2005.10.070, 2006.
- Munger, J. W., Jacob, D. J., Daube, B. C., Horowitz, L. W., Keene, W. C., and Heikes, B. G.: Formaldehyde, glyoxal, and methylglyoxal in air and cloudwater at a rural mountain site in Central Virginia, *J. Geophys. Res.*, 100, 9325–9333, doi:10.1029/95JD00508, 1995.
- Myriokefalitakis, S., Vrekoussis, M., Tsigaridis, K., Wittrock, F., Richter, A., Brühl, C., Volkamer, R., Burrows, J. P., and Kanakidou, M.: The influence of natural and anthropogenic secondary sources on the glyoxal global distribution, *Atmos. Chem. Phys.*, 8, 4965–4981, doi:10.5194/acp-8-4965-2008, 2008.
- Pikelnaya, O., Hurlock, S. C., Trick, S., and Stutz, J.: Intercomparison of multi-axis and long-path differential optical absorption spectroscopy measurements in the marine boundary layer, *J. Geophys. Res.*, 112, D10S01, doi:10.1029/2006jd007727, 2007.
- Platt, U., Marquard, L., Wagner, T., and Perner, D.: Corrections for zenith scattered light DOAS, *Geophys. Res. Lett.*, 24, 1759–1762, doi:10.1029/97gl01693, 1997.
- Possanzini, M., Tagliacozzo, G., and Cecinato, A.: Ambient levels and sources of lower carbonyls at Montelibretti, Rome (Italy), *Water Air Soil Poll.*, 183, 447–454, doi:10.1007/s11270-007-9393-1, 2007.
- Press, W. H., Teukolsky, S. A., Vetterling, W. T., and Flannery, B. P. (Eds.): Modeling of data, chap. 15, in: *Numerical Recipes – The Art of Scientific Computing*, 3rd edn., Cambridge University Press, The Edinburgh Building, Cambridge CB2 8RU, UK, 773–815, 2007.
- Richter, A., Burrows, J. P., Nusz, H., Granier, C., and Niemeier, U.: Increase in tropospheric nitrogen dioxide over China observed from space, *Nature*, 437, 129–132, doi:10.1038/nature04092, 2005.
- Rodgers, C. D.: *Inverse Methods for Atmospheric Sounding: Theory and Practice*, vol. 2 of *Atmospheric, Oceanic and Planetary Physics*, World Scientific, Hackensack, NJ, USA, 2000.
- Rothman, L. S., Jacquemart, D., Barbe, A., Chris Benner, D., Birk, M., Brown, L. R., Carleer, M. R., Chackerian, J. C., Chance, K., Coudert, L. H., Dana, V., Devi, V. M., Flaud, J. M., Gamache, R. R., Goldman, A., Hartmann, J. M., Jucks, K. W., Maki, A. G., Mandin, J. Y., Massie, S. T., Orphal, J., Perrin, A., Rinsland, C. P., Smith, M. A. H., Tennyson, J., Tolchenov, R. N., Toth, R. A., Vander Auwera, J., Varanasi, P., and Wagner, G.: The HITRAN 2004 molecular spectroscopic database, *J. Quant. Spectrosc. Ra.*, 96, 139–204, doi:10.1016/j.jqsrt.2004.10.008, 2005.
- Schauer, J. J., Kleeman, M. J., Cass, G. R., and Simoneit, B. R. T.: Measurement of emissions from air pollution sources. 2. C<sub>1</sub> through C<sub>30</sub> organic compounds from medium duty diesel trucks, *Environ. Sci. Technol.*, 33, 1578–1587, doi:10.1021/es980081n, 1999.
- Schauer, J. J., Kleeman, M. J., Cass, G. R., and Simoneit, B. R. T.: Measurement of Emissions from Air Pollution Sources. 3. C<sub>1</sub>–C<sub>29</sub> organic compounds from fireplace combustion of wood, *Environ. Sci. Technol.*, 35, 1716–1728, doi:10.1021/es001331e, 2001.
- Schauer, J. J., Kleeman, M. J., Cass, G. R., and Simoneit, B. R. T.: Measurement of emissions from air pollution sources. 5. C<sub>1</sub>–C<sub>32</sub> organic compounds from gasoline-powered motor vehicles, *Environ. Sci. Technol.*, 36, 1169–1180, doi:10.1021/es0108077, 2002.
- Sinreich, R., Volkamer, R., Filsinger, F., Frieß, U., Kern, C., Platt, U., Sebastián, O., and Wagner, T.: MAX-DOAS detection of glyoxal during ICARTT 2004, *Atmos. Chem. Phys.*, 7, 1293–130, doi:10.5194/acp-7-1293-2007, 2007.
- Stull, R. B.: *An introduction to boundary layer meteorology*, Atmospheric and Oceanographic Sciences Library, Kluwer Academic Publishers, Dordrecht, The Netherlands, 450–451, 1988.
- Takegawa, N., Miyakawa, T., Kondo, Y., Jimenez, J. L., Zhang, Q., Worsnop, D. R., and Fukuda, M.: Seasonal and diurnal variations of submicron organic aerosol in Tokyo observed using the Aerodyne aerosol mass spectrometer, *J. Geophys. Res.*, 111, D11206, doi:10.1029/2005jd006515, 2006.
- Theys, N., Van Roozendaal, M., Hendrick, F., Fayt, C., Hermans, C., Baray, J.-L., Goutail, F., Pommereau, J.-P., and De Mazière, M.: Retrieval of stratospheric and tropospheric BrO columns from multi-axis DOAS measurements at Reunion Island (21° S, 56° E), *Atmos. Chem. Phys.*, 7, 4733–4749, doi:10.5194/acp-7-4733-2007, 2007.
- Voigt, S., Orphal, J., Bogumil, K., and Burrows, J. P.: The temperature dependence (203–293 K) of the absorption cross sections of O<sub>3</sub> in the 230–850 nm region measured by Fourier-transform spectroscopy, *J. Photoch. Photobio. A*, 143, 1–9, doi:10.1016/s1010-6030(01)00480-4, 2001.
- Voigt, S., Orphal, J., and Burrows, J. P.: The temperature and pressure dependence of the absorption cross-sections of NO<sub>2</sub> in the 250–800 nm region measured by Fourier-transform spectroscopy, *J. Photoch. Photobio. A*, 149, 1–7, doi:10.1016/s1010-6030(01)00650-5, 2002.
- Volkamer, R., Spietz, P., Burrows, J., and Platt, U.: High-resolution absorption cross-section of glyoxal in the UV-vis and IR spectral ranges, *J. Photoch. Photobio. A*, 172, 35–46, doi:10.1016/j.jphotochem.2004.11.011, 2005.
- Vrekoussis, M., Wittrock, F., Richter, A., and Burrows, J. P.: Temporal and spatial variability of glyoxal as observed from space, *Atmos. Chem. Phys.*, 9, 4485–4504, doi:10.5194/acp-9-4485-2009, 2009.
- Vrekoussis, M., Wittrock, F., Richter, A., and Burrows, J. P.: GOME-2 observations of oxygenated VOCs: what can we learn from the ratio glyoxal to formaldehyde on a global scale?, *Atmos. Chem. Phys.*, 10, 10145–10160, doi:10.5194/acp-10-10145-2010, 2010.
- Wagner, T., Burrows, J. P., Deutschmann, T., Dix, B., von Friedeburg, C., Frieß, U., Hendrick, F., Heue, K.-P., Irie, H., Iwabuchi, H., Kanaya, Y., Keller, J., McLinden, C. A., Oetjen, H., Palazzi, E., Petritoli, A., Platt, U., Postlyakov, O., Pukite, J., Richter, A., van Roozendaal, M., Rozanov, A., Rozanov, V., Sinreich, R., Sanghavi, S., and Wittrock, F.: Comparison of box-air-mass-factors and radiances for Multiple-Axis Differential Opti-

- cal Absorption Spectroscopy (MAX-DOAS) geometries calculated from different UV/visible radiative transfer models, *Atmos. Chem. Phys.*, 7, 1809–1833, doi:10.5194/acp-7-1809-2007, 2007.
- Wagner, T., Beirle, S., Brauers, T., Deutschmann, T., Friß, U., Hak, C., Halla, J. D., Heue, K. P., Junkermann, W., Li, X., Platt, U., and Pundt-Gruber, I.: Inversion of tropospheric profiles of aerosol extinction and HCHO and NO<sub>2</sub> mixing ratios from MAX-DOAS observations in Milano during the summer of 2003 and comparison with independent data sets, *Atmos. Meas. Tech.*, 4, 2685–2715, doi:10.5194/amt-4-2685-2011, 2011.
- Wang, X., Zhang, Y., Hu, Y., Zhou, W., Lu, K., Zhong, L., Zeng, L., Shao, M., Hu, M., and Russell, A. G.: Process analysis and sensitivity study of regional ozone formation over the Pearl River Delta, China, during the PRIDE-PRD2004 campaign using the Community Multiscale Air Quality modeling system, *Atmos. Chem. Phys.*, 10, 4423–4437, doi:10.5194/acp-10-4423-2010, 2010.
- Wilmouth, D. M., Hanisco, T. F., Donahue, N. M., and Anderson, J. G.: Fourier transform ultraviolet spectroscopy of the  $A^2\Pi_{3/2} \leftarrow X^2\Pi_{3/2}$  transition of BrO, *J. Phys. Chem. A*, 103, 8935–8945, doi:10.1021/jp991651o, 1999.
- Wittrock, F., Oetjen, H., Richter, A., Fietkau, S., Medeke, T., Rozanov, A., and Burrows, J. P.: MAX-DOAS measurements of atmospheric trace gases in Ny-Ålesund – Radiative transfer studies and their application, *Atmos. Chem. Phys.*, 4, 955–966, doi:10.5194/acp-4-955-2004, 2004.
- Wittrock, F., Richter, A., Oetjen, H., Burrows, J. P., Kanakidou, M., Myriokefalitakis, S., Volkamer, R., Beirle, S., Platt, U., and Wagner, T.: Simultaneous global observations of glyoxal and formaldehyde from space, *Geophys. Res. Lett.*, 33, L16804, doi:10.1029/2006gl026310, 2006.
- Xiao, R., Takegawa, N., Zheng, M., Kondo, Y., Miyazaki, Y., Miyakawa, T., Hu, M., Shao, M., Zeng, L., Gong, Y., Lu, K., Deng, Z., Zhao, Y., and Zhang, Y. H.: Characterization and source apportionment of submicron aerosol with aerosol mass spectrometer during the PRIDE-PRD 2006 campaign, *Atmos. Chem. Phys.*, 11, 6911–6929, doi:10.5194/acp-11-6911-2011, 2011.
- Yue, D. L., Hu, M., Wu, Z. J., Guo, S., Wen, M. T., Nowak, A., Wehner, B., Wiedensohler, A., Takegawa, N., Kondo, Y., Wang, X. S., Li, Y. P., Zeng, L. M., and Zhang, Y. H.: Variation of particle number size distributions and chemical compositions at the urban and downwind regional sites in the Pearl River Delta during summertime pollution episodes, *Atmos. Chem. Phys.*, 10, 9431–9439, doi:10.5194/acp-10-9431-2010, 2010.
- Zhang, Y. H., Hu, M., Shao, M., Brauers, T., Chang, C. C., Hofzumahaus, A., Holland, F., Li, X., Lu, K., Kita, K., Kondo, Y., Nowak, A., Pöschl, U., Rohrer, F., Zeng, L., Wiedensohler, A., and Wahner, A.: Continuous efforts to investigate regional air pollution in the Pearl River Delta, China: PRIDE-PRD2006 campaign, *Atmos. Chem. Phys. Discuss.*, in preparation, 2012.
- Zheng, J., Zhang, L., Che, W., Zheng, Z., and Yin, S.: A highly resolved temporal and spatial air pollutant emission inventory for the Pearl River Delta region, China and its uncertainty assessment, *Atmos. Environ.*, 43, 5112–5122, doi:10.1016/j.atmosenv.2009.04.060, 2009.
- Zhou, X. and Mopper, K.: Apparent partition coefficients of 15 carbonyl compounds between air and seawater and between air and freshwater; implications for air-sea exchange, *Environ. Sci. Technol.*, 24, 1864–1869, doi:10.1021/es00082a013, 1990.